

A Lack of Evidence for Global Ram-Pressure Induced Star Formation in the Merging Cluster Abell 3266

Mark J. Henriksen, Scott Dusek

Physics Department, University of Maryland, Baltimore, MD, USA

Email: henrikse@umbc.edu

How to cite this paper: Henriksen, M.J. and Dusek, S. (2021) A Lack of Evidence for Global Ram-Pressure Induced Star Formation in the Merging Cluster Abell 3266. *International Journal of Astronomy and Astrophysics*, 11, 95-132.

<https://doi.org/10.4236/ijaa.2021.111007>

Received: January 30, 2021

Accepted: March 23, 2021

Published: March 26, 2021

Copyright © 2021 by author(s) and Scientific Research Publishing Inc. This work is licensed under the Creative Commons Attribution International License (CC BY 4.0).

<http://creativecommons.org/licenses/by/4.0/>



Open Access

Abstract

Interaction between the intracluster medium and the interstellar media of galaxies via ram-pressure stripping (RPS) has ample support from both observations and simulations of galaxies in clusters. Some, but not all of the observations and simulations show a phase of increased star formation compared to normal spirals. Examples of galaxies undergoing RPS induced star formation in clusters experiencing a merger have been identified in high resolution optical images supporting the existence of a star formation phase. We have selected Abell 3266 to search for ram-pressure induced star formation as a *global* property of a merging cluster. Abell 3266 ($z = 0.0594$) is a high mass cluster that features a high velocity dispersion, an infalling subcluster near to the line of sight, and a strong shock front. These phenomena should all contribute to making Abell 3266 an optimum cluster to see the global effects of RPS induced star formation. Using archival X-ray observations and published optical data, we cross-correlate optical spectral properties ([OII, H β]), indicative of starburst and post-starburst, respectively with ram-pressure, ρv^2 , calculated from the X-ray and optical data. We find that post-starburst galaxies, classified as E + A, occur at a higher frequency in this merging cluster than in the Coma cluster and at a comparable rate to intermediate redshift clusters. This is consistent with increased star formation due to the merger. However, both starburst and post-starburst galaxies are equally likely to be in a low or high ram pressure environment. From this result, we infer that the duration of the starburst phase must be very brief so that: 1) at any time only a small fraction of the galaxies in a high ram pressure environment show this effect, and 2) most post-starburst galaxies are in an environment of low ram pressure due to their continued orbital motion in the cluster.

Keywords

X-Ray, High Energy, Galaxy Evolution, Clusters of Galaxies

1. Introduction

An estimated 20% of all galaxies are in clusters of galaxies [1]. These large structures are typically ~ 3 million light years or more in radius and are roughly circular in projection. A hot (10^{7-8} K), X-ray emitting intracluster medium (ICM) permeates all galaxy clusters. The X-ray spectra from the plasma have a thermal bremsstrahlung continuum with emission lines from high ionization states of elements such as O, Fe, Si, and S. These elements are formed in stars and their presence in the ICM implies a connection to star formation, which takes place predominately in galaxies [2]. The elements have an average global abundance of 0.3 Solar for rich clusters with $kT \sim 5$ keV [3]. However, cluster radial metallicity profiles show a central peak of Fe as well as other elements [4]. While studies of sedimentation of metals to the center of the cluster could account, at least in part, for the excess metals [5], inclusion of the intracluster magnetic field gives a prohibitively long time for this process [6]. With the expected slow settling time via diffusive models and inhibition from a likely non-radial magnetic field, sedimentation would be inefficient. Therefore, much of the metal enhancement must have originated from local galaxy evolutionary processes that are more efficient in the cluster center. [7] originally suggested that as galaxies move through the ICM, there is a possibility that their interstellar medium (ISM) could be removed through RPS. The high velocity of the galaxy through the ICM and the local density of the ICM, which increases toward the center, results in a ram pressure that is higher in the inner 500 kpc than the outer parts of the cluster [8]. The increased metals in a region of generally higher gas density (and therefore higher ram-pressure) are consistent with RPS being associated with the metal enrichment. Though there are competing galaxy evolutionary processes that favor the cluster center [9], images of gas removal in galaxies by RPS are evident in the jelly-fish galaxies.

Modeling ram-pressure stripping of the hot coronae of galaxies in clusters is consistent with the trend of smaller cluster galaxy coronae compared to the hot X-ray halos of field galaxies. This indicates that at least some gas removal occurs within cluster environments for recently accreted galaxies [10]. In fact, evidence of ram-pressure stripping of M86 in the Virgo cluster was seen in the X-ray soon after it was predicted [11]. Later observations mapped the structure of its 150 kpc tidal tail in the X-ray with high resolution [12] providing details of the stripping process. More recently, an ample number of observations showing that RPS occurs in galaxy clusters [13] [14] [15] have become available. Simulations and observations generally agree that the outer disk (>20 kpc) is stripped first and the gas forms a tail in the wake of the galaxy [16]-[21]. Simulations are in general agreement that ram pressure increases the galactic star formation rate [22] [23] and there are examples of increased star formation observed during RPS [24] [25] [26] [27] [28]. [27] reports a significant enhancement in star formation due to RPS in a large sample of clusters using optical spectroscopy. However, there are counter examples of RPS where enhanced star formation is

not seen; for example, in the Virgo cluster [29].

A general feature of simulations that are characterized by enhanced star formation is that ram pressure causes a compression of the gas within the disk of the galaxy. This transfer of gas from the outer regions of the galaxy to the inner, increases the gas density, resulting in an increase in the star formation rate. However, other simulations do not see enhanced star formation in the disk [30] or only a slight enhancement for galaxies with select physical parameters and orientation [31] [32] [33]. Simulations of RPS during a galaxy cluster merger [22] [23] show increased star formation due to local enhancements in gas density from the cluster wide shocks that typically accompany mergers and the broadened velocity dispersion. This phase of enhanced star formation in the disk and gas halo stripping [34] leads to an overall reduction of the gas available to the galaxy, resulting in a subsequent decrease in the overall star formation rate. Thus, there is an optimum time to observe the increased star formation rate as it should only be enhanced for a relatively short time period after ram pressure stripping begins [22]. The length of time depends on the strength of the ram pressure acting on the galaxy and the velocity of the galaxy, since this would affect the length of the RPS phase. As the galaxy encounters denser regions of the ICM, and hence stronger ram pressure, higher star formation rates should occur. This is directly observed in the Jellyfish galaxies found in merging clusters [35] [36] [37]; [26]. The increase in star formation should be accompanied by an observed enhancement in the equivalent width of emission or absorption lines. The stripping timescale in the center of the cluster is estimated at 200 - 500 Myr [33] [16] [8] so that if a galaxy cluster is observed after this time, any enhancement in these lines may no longer be observable.

[27] has reported increased star formation via RPS in clusters of various morphology using a spectroscopic data set. In this paper, we will specifically address the connection with cluster merger. We have chosen a cluster with an ongoing merger to look for a global effect of increased star formation since there is some disagreement about the importance of this phase in the simulations. Abell 3266 is a well studied cluster with an ongoing merger [38] [39] [40] [41]. The cluster has a high velocity dispersion in the central region, $1367 \text{ km}\cdot\text{s}^{-1}$, while the outer region of the cluster exhibits a velocity dispersion similar to other rich clusters, $1000 \text{ km}\cdot\text{s}^{-1}$ [39]. These velocities are consistent with the trend in values derived by [41] though smaller as these authors use a less restrictive velocity criterion for cluster membership and therefore model the larger cluster environment. The merger process creates more high velocity galaxies in the cluster as the kinetic energy of the infalling subcluster is turned into internal cluster energy via dynamical friction thus inflating the velocity dispersion in the central region. The cluster velocity distribution also has a high velocity component identified with a subcluster, which contains 30 galaxies [40]. Further evidence of a merger is an asymmetric gas distribution and regions of shocked gas [39]. There should be higher ram pressure in these local regions of increased galaxy velocity

and post-shock, higher density gas. Depending on the timescale of stripping, as discussed above, we expect to see a correlation between high local ram pressure and the equivalent width of [OII] or H β due to an increase in star formation. If no correlation is seen between ram pressure and these lines, it could be that this phase of star formation has already ceased. However, a cluster with an ongoing merger is the best case for catching the relatively short duration process of induced star formation.

2. X-Ray and Optical Data

Abell 3266 is a galaxy cluster located in the Southern Hemisphere at 4h31m24.1s, $-61^{\circ}26'38.0''$ (J2000) at a redshift of $z = 0.0594$ [41]. X-ray observations showed a central temperature enhancement in the intracluster medium, possibly due to a merger [42]. A detailed temperature map confirmed the merger and provided details of the shock structure as well as the geometry of the merger [39]. The extended cluster region shows a complex gas [38] and optical structure containing six groups and filaments to the north of the cluster [41]. Abell 3266 was observed with the ROSAT Position-Sensitive Proportional Counter (PSPC), for 13,547 seconds between August 19, 1993 to September 27, 1993. We choose to use the ROSAT PSPC over higher resolution data sets because its large field of view, 2 degrees, matches the cluster size and provides full coverage of the Abell 3266 cluster. The position, velocity, and equivalent width of H β and [OII] for each galaxy were obtained from the Wide-Field Nearby Galaxy Clusters Survey [43]. The spectroscopic data given in **Table 1** is from [44]. Typically, the equivalent width of H α is used as an optical indicator of recent star formation [45]. When the spectroscopic data collected for Abell 3266 was fit, the H α line was found to be in a cluttered region of the spectrum. This is due to the presence of the NII spectral lines, at wavelengths of 6548Å and 6583Å, on either side of the H α line. The uncertainty in the H α line for this cluster lead us to choose the H β line as the preferred indicator of star formation. When examining the intensity of the Balmer series transitions, the ratio of intensity of H α compared to H β at 10,000 K is 2.87, and all subsequent Balmer transitions higher than H β are substantially weaker. So, although H α could not be used for this study, H β is a reasonable alternative for detecting star formation since it is the next strongest Balmer line. The [OII] emission is due to hot, young stars, namely O and B type stars. The optimal conditions for producing [OII] emission can be found in HII regions [46]. Because of the short lifetime for these massive stars, [OII] emission is a good indicator of the most recent star formation.

There are other star formation indicators than those used here and indicators exist across the electromagnetic spectrum, including: radio line and continuum, FIR, optical emission and absorption lines, UV, and X-ray. Each indicator has advantages and disadvantages with regard to applicability and calibration (see references in [45]). Indicators in the UV/optical/NIR rely on radiation from the stars themselves, while the FIR, radio, and X-ray are less direct. The radio

Table 1. Optical Line Equivalent Widths.

WINGS ID	[OII] EW Width (Å)	[OII EW] Error Width (Å)	H δ EW Width (Å)	H δ EW Error Width (Å)	H β EW Width (Å)	H β EW Error Width (Å)	RA Degrees	DEC Degrees
J042847.65-613052.9	–	–	2.16	0.81	0.87	0.58	67.19854	-61.51469
J042856.57-613753.8	–	–	7.98	2.27	0.29	0.34	67.23571	-61.63161
J042902.02-611354.9	–	–	2.2	1.15	2.88	1.15	67.25842	-61.23192
J042902.33-612417.2	-9.37	2.59	5.29	1.25	-2.02	0.86	67.25971	-61.40478
J042905.27-611302.4	-10.72	2.79	3.77	1.16	-7.76	1.7	67.27196	-61.21733
J042905.22-611321.7	-17.76	2.54	7	1.79	-6	1.42	67.27175	-61.22269
J042907.20-612018.3	–	–	1.03	0.6	2.55	0.88	67.28	-61.33842
J042908.67-613906.4	-9.96	6.86	-2.81	1.04	1.92	0.86	67.28612	-61.65178
J042912.95-611508.4	-35.65	8.31	4.76	1.28	1.67	0.69	67.30396	-61.25233
J042916.95-611953.1	-11.09	1.9	1.82	1.16	-4.08	1.96	67.32062	-61.33142
J042917.68-612818.2	–	–	1.06	0.63	1.41	0.71	67.32367	-61.47172
J042918.62-611929.8	–	–	1.83	0.8	0.84	0.49	67.32758	-61.32494
J042918.93-611419.3	–	–	3.08	1.11	1.29	0.68	67.32887	-61.23869
J042924.75-611905.7	–	–	0.79	0.51	1.99	0.7	67.35312	-61.31825
J042924.92-612603.4	–	–	0.92	0.56	1.3	0.6	67.35383	-61.43428
J042925.36-613345.9	–	–	0.83	0.68	0.73	0.53	67.35567	-61.56275
J042926.28-611155.9	0	0.56	4.16	1.25	0.82	0.59	67.3595	-61.19886
J042927.18-611651.9	-2.93	2.1	3.48	1.11	2.4	0.76	67.36325	-61.28108
J042927.89-612337.0	–	–	1.44	0.71	2.45	0.91	67.36621	-61.39361
J042932.77-611452.5	–	–	0.44	0.38	1.46	0.72	67.38654	-61.24792
J042933.01-611124.4	-2.18	1.31	2.47	0.92	-1.02	1.08	67.38754	-61.19011
J042933.10-611536.3	-2.55	1.53	1.73	0.77	0.74	0.46	67.38792	-61.26008
J042934.78-612803.7	–	–	1.05	0.6	1.59	0.73	67.39492	-61.46769
J042936.13-611450.2	–	–	–	–	2.48	1.13	67.40054	-61.24728
J042937.98-611445.5	–	–	1.2	0.66	2.41	0.92	67.40825	-61.24597
J042939.59-611034.5	-30.48	5.48	-0.24	0.27	-1.58	0.78	67.41496	-61.17625
J042944.51-611456.3	-17.76	3.3	2.31	0.82	-10.04	1.99	67.43546	-61.24897
J042944.77-613054.9	–	–	2.68	1.05	2.83	1.05	67.43654	-61.51525
J042946.91-613025.6	-31.43	8.41	-7.68	1.45	6.02	1.59	67.44546	-61.50711
J042947.62-612337.0	–	–	–	–	7.11	3.14	67.44842	-61.39361
J042948.73-613732.2	–	–	–	–	2.44	0.87	67.45304	-61.62561
J042951.03-611127.3	–	–	1.38	0.69	1.55	0.72	67.46262	-61.19092
J042951.96-611812.9	-4.13	1.43	–	–	0.36	0.42	67.4665	-61.30358
J042957.45-611145.7	–	–	1.26	0.72	2.57	0.98	67.48937	-61.19603
J043000.74-612554.3	-21.87	16.42	2.23	1.08	1.98	1.07	67.50308	-61.43175

Continued

J043003.09-611714.0	-22.73	8.03	2.3	1.13	0.89	0.96	67.51287	-61.28722
J043003.77-611555.4	-	-	0.27	0.38	0.14	0.33	67.51571	-61.26539
J043004.38-612255.5	-	-	3.78	1.13	2.32	1.06	67.51825	-61.38208
J043004.47-612325.7	0	0.7	2.56	0.95	1.52	0.73	67.51862	-61.39047
J043006.99-613551.2	-	-	5.8	1.79	4.2	1.49	67.52912	-61.59756
J043007.64-612003.6	0	0.49	1.08	0.67	2.25	0.92	67.53183	-61.33433
J043008.03-611809.3	-30.83	7.46	0.02	0.14	-1.23	1.24	67.53346	-61.30258
J043008.45-612529.8	-	-	-	-	3.78	1.94	67.53521	-61.42494
J043012.30-611946.4	-	-	-	-	-6.82	2.85	67.55125	-61.32956
J043014.66-612808.7	-	-	7.34	1.47	3.29	1	67.56108	-61.46908
J043014.72-613145.4	-	-	-	-	1.75	0.87	67.56133	-61.52928
J043016.68-612239.4	-	-	-	-	3.02	1.9	67.5695	-61.37761
J043017.05-611844.1	-46.92	5.74	4.78	1.25	-8.07	1.71	67.57104	-61.31225
J043018.11-613508.8	-3.17	1.14	2.2	0.87	-2.12	0.84	67.57546	-61.58578
J043018.94-611806.9	-	-	5.39	1.48	0.41	0.53	67.57892	-61.30192
J043020.03-612609.7	-	-	3.09	1.18	2.48	1.02	67.58346	-61.43603
J043021.56-612848.7	0	0.25	1.44	0.68	1.24	0.66	67.58983	-61.48019
J043022.67-612319.6	-12.71	5.45	4.67	1.38	1.3	0.68	67.59446	-61.38878
J043025.99-612745.9	-	-	5.28	2.55	-4.79	1.8	67.60829	-61.46275
J043026.05-613524.8	-35.58	18.78	-12.89	1.98	2.69	0.94	67.60854	-61.59022
J043026.74-613031.9	-4.99	2.82	1.71	0.83	2.82	1.09	67.61142	-61.50886
J043026.85-613503.1	-	-	8.14	1.93	7.24	2.18	67.61187	-61.58419
J043028.36-611704.0	-17.28	5.12	1.49	0.86	0.43	0.74	67.61817	-61.28444
J043028.68-611939.8	-	-	-	-	0.49	0.46	67.6195	-61.32772
J043028.84-613932.5	-	-	2.92	1.19	2.58	1	67.62017	-61.65903
J043030.43-612023.1	-3.23	1.61	2.89	1.02	0.51	0.46	67.62679	-61.33975
J043032.07-614200.6	-25.8	8.63	0.03	0.48	-7.23	1.69	67.63362	-61.70017
J043032.53-611257.5	-	-	2.46	1	0.67	0.82	67.63554	-61.21597
J043032.85-613755.5	-	-	1.42	0.73	1.69	0.92	67.63687	-61.63208
J043033.23-613300.7	-	-	4.77	2.09	8.44	2.63	67.63846	-61.55019
J043034.31-611912.6	-	-	2.3	1.17	1.86	1.05	67.64296	-61.32017
J043037.57-614249.6	-	-	1.85	0.97	6.42	2.62	67.65654	-61.71378
J043037.69-612902.7	-	-	1.47	0.75	1.28	0.74	67.65704	-61.48408
J043038.92-612837.5	-	-	2.14	0.94	3.38	1.42	67.66217	-61.47708
J043039.53-613507.8	-	-	2.2	0.9	1.39	0.66	67.66471	-61.5855
J043039.66-611751.9	-3.47	2.26	2.74	1.11	8.73	1.88	67.66525	-61.29775
J043041.79-612243.1	-3.15	1.78	1.37	0.6	1.76	0.75	67.67412	-61.37864

Continued

J043041.87-612715.8	0	0.6	0.91	0.54	2.7	0.81	67.67446	-61.45439
J043041.86-611303.0	-	-	1.95	0.84	2.8	1.02	67.67442	-61.2175
J043041.88-611709.9	-	-	-	-	2.05	0.82	67.6745	-61.28608
J043043.25-612106.9	-66.91	7.36	-	-	-18.85	2.49	67.68021	-61.35192
J043044.89-611104.6	-	-	-	-	1.5	0.85	67.68704	-61.18461
J043045.32-613300.4	-	-	4.22	1.41	1.5	0.83	67.68883	-61.55011
J043045.38-612335.7	0	0.37	1.38	0.63	0.54	0.37	67.68908	-61.39325
J043045.64-613538.7	-	-	0.69	0.63	2.09	1.32	67.69017	-61.59408
J043046.27-611132.2	-	-	-	-	1.25	0.61	67.69279	-61.19228
J043050.16-611543.9	0	0.09	1.5	0.71	1.9	0.8	67.709	-61.26219
J043050.35-611406.0	0	1.18	-	-	1.53	1.03	67.70979	-61.235
J043051.24-611059.7	0	0.26	1.07	0.52	0.94	0.55	67.7135	-61.18325
J043051.87-612324.4	-	-	3.13	1.16	6.89	1.64	67.71612	-61.39011
J043052.13-611034.7	-	-	-	-	-0.73	0.83	67.71721	-61.17631
J043052.25-612813.8	-	-	1.89	0.77	0.59	0.46	67.71771	-61.4705
J043053.08-612514.2	-3.05	2.26	4.28	1.13	3.2	1.57	67.72117	-61.42061
J043053.73-613005.7	-	-	1.65	0.77	2.3	0.83	67.72387	-61.50158
J043054.21-612103.2	-	-	2.05	0.82	1.48	0.69	67.72587	-61.35089
J043055.49-612014.3	-	-	2.27	1.13	2.01	0.98	67.73121	-61.33731
J043056.84-613202.3	-	-	1.53	0.71	1.74	0.71	67.73683	-61.53397
J043056.87-611333.5	-	-	3.31	1.22	3.79	1.55	67.73696	-61.22597
J043056.90-612147.4	-	-	3.66	1.34	-2.01	1.67	67.73708	-61.36317
J043057.00-613107.3	-11.63	6.7	-19.85	2.91	6.8	2.09	67.7375	-61.51869
J043058.25-613536.2	-5.99	3.96	0.73	0.47	0.21	0.54	67.74271	-61.59339
J043058.75-611021.0	-	-	-	-	-1.28	0.8	67.74479	-61.1725
J043059.59-612507.2	-	-	-	-	1.04	0.79	67.74829	-61.41867
J043059.55-612740.1	-9.39	8.53	6.53	1.61	-9.28	4.98	67.74812	-61.46114
J043059.77-613438.5	0	0.17	1.19	0.71	1.76	0.89	67.74904	-61.57736
J043100.91-612957.9	-57.74	12.48	-	-	-5.96	4.46	67.75379	-61.49942
J043104.72-613053.4	-	-	5.42	1.52	-0.7	1.02	67.76967	-61.51483
J043104.61-612802.6	-	-	1.21	0.57	1.71	0.67	67.76921	-61.46739
J043107.70-613012.1	-	-	3.53	1.35	-0.46	0.78	67.78208	-61.50336
J043108.34-613413.8	-	-	4.39	1.36	1.17	1.01	67.78475	-61.5705
J043108.71-612707.0	-2.82	2.08	2.41	0.94	1.69	1.01	67.78629	-61.45194
J043108.81-612510.1	-24.6	7.22	3.67	1.01	-6.88	1.45	67.78671	-61.41947
J043109.75-612535.8	-	-	-	-	5.96	1.83	67.79062	-61.42661
J043112.64-612728.9	0	0.29	1.12	0.68	1.75	0.76	67.80267	-61.45803

Continued

J043113.20-611037.9	–	–	–	–	0.64	0.65	67.805	–61.17719
J043114.59-612344.7	0	1.49	1.97	1.09	1.83	0.95	67.81079	–61.39575
J043117.02-612724.2	–	–	7.41	1.76	1.08	1.15	67.82092	–61.45672
J043117.25-613149.8	–2.3	1.69	6.24	1.29	3.62	1.09	67.82187	–61.5305
J043117.66-612743.7	–	–	–	–	3.37	1.2	67.82358	–61.46214
J043121.54-613016.3	–	–	–	–	–0.85	1.14	67.83975	–61.50453
J043121.86-612517.7	–	–	0.93	0.93	0.56	0.74	67.84108	–61.42158
J043123.30-612726.9	–	–	1.31	0.65	0.52	0.42	67.84708	–61.45747
J043126.94-612301.3	–5.97	2.29	8.25	1.62	4.28	1.07	67.86225	–61.38369
J043130.61-613845.0	–26.95	4.34	2.65	0.89	–1.86	1.07	67.87754	–61.64583
J043131.08-614208.8	–	–	1.53	1.03	3.91	1.49	67.8795	–61.70244
J043137.44-612552.9	–	–	–	–	3.12	0.99	67.906	–61.43136
J043139.30-613951.6	–	–	–	–	–4.61	1.81	67.91375	–61.66433
J043139.39-612141.8	–23.83	5.01	2.83	1.19	–0.58	0.91	67.91412	–61.36161
J043140.34-611635.3	–	–	2.57	0.99	1.62	0.73	67.91808	–61.27647
J043142.26-613139.2	0	0.32	0.09	0.18	0.67	0.46	67.92608	–61.52756
J043142.88-613020.1	–	–	1.81	0.87	1.32	0.75	67.92867	–61.50558
J043147.43-611754.8	–18.34	2.78	5.71	1.39	–17.05	2.94	67.94762	–61.29856
J043148.16-611802.1	–	–	5.93	1.8	3.92	1.72	67.95067	–61.30058
J043148.33-611633.8	–	–	8.23	1.52	1.53	1.39	67.95137	–61.27606
J043150.03-611929.7	–10.85	4.49	7.57	1.73	3.58	1.43	67.95846	–61.32492
J043150.25-613046.3	–	–	0.55	0.44	0.94	0.72	67.95937	–61.51286
J043151.90-613215.1	–	–	–	–	–3.58	3.32	67.96625	–61.53753
J043153.18-611850.0	–	–	–	–	8.37	2.34	67.97158	–61.31389
J043153.46-612941.2	–	–	5.97	1.54	2.36	1.1	67.97275	–61.49478
J043153.58-612738.5	–	–	6.31	1.58	0.78	1.18	67.97325	–61.46069
J043153.72-612614.4	–	–	–	–	2.32	0.86	67.97383	–61.43733
J043155.17-613042.0	–63.03	13.55	–1.44	0.74	–15.67	3.41	67.97987	–61.51167
J043158.70-611624.1	–8.26	3.93	1.63	0.69	1.63	0.67	67.99458	–61.27336
J043200.75-611503.0	–	–	2.8	0.97	1.23	0.78	68.00312	–61.25083
J043202.49-611946.6	–	–	1.98	0.87	1.68	0.81	68.01037	–61.32961
J043212.83-611232.9	–	–	2.56	0.94	2.21	0.93	68.05346	–61.20914
J043213.28-612540.2	–5.97	3.25	3.8	1.38	2.81	1.03	68.05533	–61.42783
J043213.90-613812.0	0	0.02	3	1.09	4.24	1.21	68.05792	–61.63667
J043218.84-611920.3	–	–	5.01	1.35	4	1.29	68.0785	–61.32231
J043221.93-611041.2	–6.94	6.72	–	–	1.82	0.88	68.09137	–61.17811
J043222.39-613551.0	–117.41	86.44	–0.55	0.77	3.47	1.1	68.09329	–61.5975

Continued

J043223.53-613340.0	–	–	0.34	0.33	1.58	0.69	68.09804	-61.56111
J043225.62-612320.0	-31.43	6.95	–	–	4.65	2.05	68.10675	-61.38889
J043226.65-612134.2	–	–	2.81	0.94	4.26	2.01	68.11104	-61.3595
J043229.88-613044.6	0	1.09	1.21	0.56	1.58	0.72	68.1245	-61.51239
J043233.84-613838.8	–	–	1.33	0.68	2.69	0.96	68.141	-61.64411
J043234.08-611359.1	-4.32	1.46	1.59	0.75	-1.46	0.73	68.142	-61.23308
J043234.77-611455.5	–	–	3.33	1.06	2.4	1.07	68.14487	-61.24875
J043235.35-612945.4	–	–	3.93	1.3	1.51	0.96	68.14729	-61.49594
J043239.62-612555.1	–	–	–	–	-4.8	2.15	68.16508	-61.43197
J043240.10-612542.5	–	–	1.21	0.62	1.67	0.74	68.16708	-61.42847
J043241.58-612303.8	-4.13	2.75	2.44	1.11	3.7	1.19	68.17325	-61.38439
J043242.82-612811.1	–	–	2.97	1.01	0.84	0.75	68.17842	-61.46975
J043244.94-611627.0	-13.95	3.89	5.41	1.2	1.14	0.79	68.18725	-61.27417
J043245.88-613256.3	–	–	–	–	2.55	1.14	68.19117	-61.54897
J043247.12-612107.2	0	0.97	3.64	1.06	3.12	1.4	68.19633	-61.352
J043247.60-612511.3	–	–	–	–	6.04	1.33	68.19833	-61.41981
J043248.45-611947.8	–	–	–	–	6.26	1.74	68.20187	-61.32994
J043252.93-612936.9	-28.85	4.2	–	–	-12.75	3.68	68.22054	-61.49358
J043254.13-612132.4	–	–	–	–	0.83	0.6	68.22554	-61.359
J043254.18-612547.7	–	–	1.8	0.73	2.22	0.95	68.22575	-61.42992
J043255.41-611910.4	0	0.25	1.68	0.7	4.01	1.06	68.23087	-61.31956
J043257.83-612547.2	–	–	1.86	0.84	2.21	0.93	68.24096	-61.42978
J043258.46-613005.1	0	0.5	1.59	0.73	2.48	0.83	68.24358	-61.50142
J043306.66-612613.7	0	0.14	0.89	0.53	1.16	0.63	68.27775	-61.43714
J043308.58-612115.4	-2.47	2.02	3.52	1.14	2.34	0.9	68.28575	-61.35428
J043309.01-612312.1	–	–	6.9	1.57	-3.14	1.81	68.28754	-61.38669
J043314.12-612034.0	–	–	2.23	0.87	1.78	0.73	68.30883	-61.34278
J043315.31-612143.0	–	–	–	–	2.04	0.79	68.31379	-61.36194
J043316.32-611800.9	-4.96	2.81	1.48	0.75	1.81	0.73	68.318	-61.30025
J043322.76-612845.8	–	–	–	–	0.43	0.4	68.34483	-61.47939

line-to-continuum ratio, involving free-free emission from a star-forming region, must be separated from contaminating dust and synchrotron emission (references in [47]). The FIR, UV, and X-ray are associated with high mass stars and therefore recent or ongoing star formation, in the last 100 million years or so. The Balmer and oxygen emission and absorption lines, used in this paper, have the advantage of covering a broader range of stellar mass, from intermediate to high and therefore cover several billion years of star formation.

However, the optical lines have the disadvantage of sensitivity to attenuation by dust.

3. Analysis

Given the large number of groups in the cluster found optically that also appear to have enhanced X-ray emission [41], we calculate the local gas density for each galaxy. The local gas density is obtained from an annulus with inner radius of 25 kpc and outer radius of 50 kpc. These values are nominally chosen to both exclude emission from a disk similar to the Milky Way and restrict gas density to the local value encountered by the galaxy. The angular scale for Abell 3266 is 70.4 kpc·arcmin⁻¹ so the annulus dimensions are sub arc minute. The point-spread function for the PSPC is described by a Gaussian with a width that varies with distance from the detector center from 15 arc sec to 50 arc sec at 1 keV [48]. Thus the regions are folded through the point spread function (see **Table 2**). The energy range for each region was restricted to 0.5 - 2.4 keV, which maximizes source counts while minimizing background contamination. Only galaxies with an X-ray signal-to-noise count rate greater than 3 were used to obtain a gas density. The count rate is converted to a flux using an APEC model with specified values for temperature, abundance, and column density. The fluxes and normalizations are shown in **Table 3**. The ion density is calculated from the normalization, which contains the emission integral, using the sampled volume and an average electron per ion corresponding to the assumed abundances. The ion density is given in **Table 4**. The abundances assumed for the count rate to flux conversion as well as the density calculation is 90% H and 10% He, with metals ignored. The emission weighted PSPC temperature, 5.8 keV [40] is used throughout the cluster as the PSPC is insensitive to temperature changes in the X-ray emitting gas. The column density is set to 2×10^{20} cm⁻² [49].

The ram pressure depends on the velocity of each galaxy in addition to the ion density and mass. [40] found that the range of galaxies in the Abell 3266, following a clipping procedure described in detail there, includes galaxies with heliocentric velocity between 15,000 and 21,000 km·s⁻¹. **Figure 1** shows the velocity histogram for the galaxies used in our analysis.

Of the original 263 galaxies in the WINGS survey, 51 are outside of the velocity range and are likely foreground or background. Another 35 galaxies are eliminated due to low signal-to-noise X-ray data or non-physical [OII] values. The heliocentric velocity of the main cluster core found by [40] is 17,804 km·s⁻¹ giving a redshift of 0.0594, consistent with [41]. We use 0.0594 as the redshift throughout the paper. The velocity of each galaxy is found by subtracting the galaxy velocity from the heliocentric cluster velocity. The galaxy velocities are given in **Table 4**. The distribution of galaxies, as seen in **Figure 1**, is asymmetric and the peak is offset from zero, further evidence of the merger.

In general, the gas density is higher toward the center, and lower in the outskirts. However, in a cluster merger, there is an asymmetry in the X-ray surface

Table 2. Regions for Gas Density Measurements.

Hour	RA			DEC		Off Axis Radius (arcmin)	PSF Width (arc sec)	Inner Radius (arcsec)	Outer Radius (arcsec)
	min	sec	degrees	arcmin	arcsec				
4	31	50.03	-61	19	29.7	12.4337	19.9201	44.9201	69.9201
4	30	34.31	-61	19	12.6	11.2017	17.973	42.973	67.973
4	30	50.16	-61	15	43.9	14.6472	23.8213	48.8213	73.8213
4	31	40.34	-61	16	35.3	14.724	23.9649	48.9649	73.9649
4	30	59.59	-61	25	7.2	4.07797	11.037	36.037	61.037
4	30	8.03	-61	18	9.3	13.7105	22.112	47.112	72.112
4	31	39.39	-61	21	41.8	9.58788	15.7072	40.7072	65.7072
4	31	13.2	-61	10	37.9	20.4041	35.8627	60.8627	85.8627
4	32	47.12	-61	21	7.2	16.8322	28.1034	53.1034	78.1034
4	33	14.12	-61	20	34	20.3085	35.644	60.644	85.644
4	32	55.41	-61	19	10.4	18.9509	32.6022	57.6022	82.6022
4	32	26.65	-61	21	34.2	14.2444	23.0761	48.0761	73.0761
4	30	28.36	-61	17	4	13.7331	22.1522	47.1522	72.1522
4	29	44.51	-61	14	56.3	18.4374	31.4832	56.4832	81.4832
4	29	57.45	-61	11	45.7	20.767	36.6974	61.6974	86.6974
4	30	56.87	-61	13	33.5	17.0372	28.5244	53.5244	78.5244
4	30	58.75	-61	10	21	20.6304	36.3822	61.3822	86.3822
4	30	51.24	-61	10	59.7	19.9349	34.7953	59.7953	84.7953
4	29	39.59	-61	10	34.5	23.0053	42.0159	67.0159	92.0159
4	30	50.35	-61	14	6	16.4688	27.3644	52.3644	77.3644
4	29	5.27	-61	13	2.4	23.3189	42.7833	67.7833	92.7833
4	30	4.47	-61	23	25.7	9.43714	15.5137	40.5137	65.5137
4	30	45.38	-61	23	35.7	6.06744	12.1249	37.1249	62.1249
4	29	18.62	-61	19	29.8	16.9995	28.4468	53.4468	78.4468
4	29	47.62	-61	23	37	11.1649	17.9177	42.9177	67.9177
4	30	22.67	-61	23	19.6	7.79429	13.6278	38.6278	63.6278
4	29	24.75	-61	19	5.7	16.6465	27.7244	52.7244	77.7244
4	30	53.08	-61	25	14.2	4.02546	11.0173	36.0173	61.0173
4	30	28.68	-61	19	39.8	10.9741	17.6329	42.6329	67.6329
4	29	32.77	-61	14	52.5	19.3951	33.5845	58.5845	83.5845
4	29	27.18	-61	16	51.9	18.1529	30.8708	55.8708	80.8708
4	31	8.71	-61	27	7	2.25179	10.5845	35.5845	60.5845
4	29	2.33	-61	24	17.2	16.4114	27.2487	52.2487	77.2487
4	29	34.78	-61	28	3.7	11.2969	18.1171	43.1171	68.1171

Continued

4	29	33.1	-61	15	36.3	18.7164	32.089	57.089	82.089
4	30	20.03	-61	26	9.7	5.97435	12.0586	37.0586	62.0586
4	29	24.92	-61	26	3.4	12.9547	20.7942	45.7942	70.7942
4	29	25.36	-61	33	45.9	13.712	22.1146	47.1146	72.1146
4	30	37.69	-61	29	2.7	2.86953	10.6878	35.6878	60.6878
4	30	14.66	-61	28	8.7	5.97325	12.0578	37.0578	62.0578
4	30	57	-61	31	7.3	2.66258	10.6481	35.6481	60.6481
4	29	48.73	-61	37	32.2	13.593	21.9034	46.9034	71.9034
4	30	52.25	-61	28	13.8	1.08041	10.4926	35.4926	60.4926
4	29	8.67	-61	39	6.4	18.74	32.1406	57.1406	82.1406
4	30	32.85	-61	37	55.5	10.8505	17.4511	42.4511	67.4511
4	30	45.32	-61	33	0.4	5.10075	11.5112	36.5112	61.5112
4	30	39.53	-61	35	7.8	7.60024	13.4335	38.4335	63.4335
4	30	18.11	-61	35	8.8	9.00532	14.9778	39.9778	64.9778
4	30	37.57	-61	42	49.6	16.0239	26.474	51.474	76.474
4	30	59.77	-61	34	38.5	6.5948	12.529	37.529	62.529
4	31	31.08	-61	42	8.8	15.6023	25.6447	50.6447	75.6447
4	31	17.25	-61	31	49.8	4.21908	11.0922	36.0922	61.0922
4	31	42.26	-61	31	39.2	6.63035	12.558	37.558	62.558
4	32	13.9	-61	38	12	14.5553	23.65	48.65	73.65
4	32	22.39	-61	35	51	13.6799	22.0574	47.0574	72.0574
4	32	33.84	-61	38	38.8	16.8205	28.0793	53.0793	78.0793
4	32	35.35	-61	29	45.4	12.934	20.759	45.759	70.759
4	32	40.1	-61	25	42.5	13.9603	22.5597	47.5597	72.5597
4	31	55.17	-61	30	42	7.81878	13.6528	38.6528	63.6528
4	32	45.88	-61	32	56.3	15.0305	24.5435	49.5435	74.5435
4	32	42.82	-61	28	11.1	13.9052	22.4605	47.4605	72.4605
4	31	23.3	-61	27	26.9	3.56717	10.8634	35.8634	60.8634
4	32	47.6	-61	25	11.3	15.0819	24.6414	49.6414	74.6414
4	32	13.28	-61	25	40.2	10.5296	16.9877	41.9877	66.9877
4	32	41.58	-61	23	3.8	15.1529	24.7769	49.7769	74.7769
4	33	9.01	-61	23	12.1	18.4975	31.6132	56.6132	81.6132
4	31	37.44	-61	25	52.9	6.07204	12.1282	37.1282	62.1282
4	33	16.32	-61	18	0.9	22.008	39.6109	64.6109	89.6109
4	31	14.59	-61	23	44.7	5.99355	12.0722	37.0722	62.0722
4	31	21.86	-61	25	17.7	4.94247	11.4263	36.4263	61.4263

Continued

4	33	6.66	-61	26	13.7	17.3227	29.1164	54.1164	79.1164
4	32	54.18	-61	25	47.7	15.7737	25.9801	50.9801	75.9801
4	33	15.31	-61	21	43	19.9006	34.7178	59.7178	84.7178
4	31	58.7	-61	16	24.1	15.999	26.4245	51.4245	76.4245
4	32	34.77	-61	14	55.5	20.1417	35.2641	60.2641	85.2641
4	32	34.08	-61	13	59.1	20.9086	37.0253	62.0253	87.0253
4	30	51.87	-61	23	24.4	6.07313	12.129	37.129	62.129
4	32	44.94	-61	16	27	19.81	34.5136	59.5136	84.5136
4	30	41.79	-61	22	43.1	7.15115	13.0081	38.0081	63.0081
4	32	12.83	-61	12	32.9	20.6981	36.5383	61.5383	86.5383
4	30	43.25	-61	21	6.9	8.82232	14.7591	39.7591	64.7591
4	30	54.21	-61	21	3.2	8.65877	14.568	39.568	64.568
4	31	8.81	-61	25	10.1	4.23185	11.0973	36.0973	61.0973
4	32	0.75	-61	15	3	17.4571	29.3971	54.3971	79.3971
4	30	17.05	-61	18	44.1	12.5641	20.1361	45.1361	70.1361
4	29	51.03	-61	11	27.3	21.4363	38.2574	63.2574	88.2574
4	30	41.88	-61	17	9.9	13.1943	21.2058	46.2058	71.2058
4	30	44.89	-61	11	4.6	19.9066	34.7315	59.7315	84.7315
4	30	41.86	-61	13	3	17.7545	30.0227	55.0227	80.0227
4	29	37.98	-61	14	45.5	19.0932	32.9156	57.9156	82.9156
4	29	32.16	-61	13	13	20.9638	37.1533	62.1533	87.1533
4	29	26.28	-61	11	55.9	22.6027	41.0383	66.0383	91.0383
4	29	2.02	-61	13	54.9	22.8824	41.7164	66.7164	91.7164
4	30	7.6	-61	20	3.6	11.939	19.1174	44.1174	69.1174
4	30	33.1	-61	24	22.6	6.01252	12.0856	37.0856	62.0856
4	29	7.2	-61	20	18.3	17.7337	29.9788	54.9788	79.9788
4	29	12.95	-61	15	8.4	20.8735	36.9438	61.9438	86.9438
4	30	59.55	-61	27	40.1	1.22339	10.4981	35.4981	60.4981
4	29	51.96	-61	18	12.9	14.8499	24.2016	49.2016	74.2016
4	29	27.89	-61	23	37	13.498	21.7356	46.7356	71.7356
4	30	3.09	-61	17	14	14.9374	24.367	49.367	74.367
4	30	30.43	-61	20	23.1	10.1359	16.4377	41.4377	66.4377
4	30	41.87	-61	27	15.8	2.84001	10.6818	35.6818	60.6818
4	29	17.68	-61	28	18.2	13.5667	21.8568	46.8568	71.8568
4	30	33.23	-61	33	0.7	5.88135	11.994	36.994	61.994
4	29	35.69	-61	31	40.7	11.6083	18.5961	43.5961	68.5961

Continued

4	30	21.56	-61	28	48.7	5.00984	11.4619	36.4619	61.4619
4	28	47.65	-61	30	52.9	17.7234	29.9569	54.9569	79.9569
4	30	53.73	-61	30	5.7	1.65623	10.5234	35.5234	60.5234
4	30	26.74	-61	30	31.9	4.75041	11.329	36.329	61.329
4	28	56.57	-61	37	53.8	19.284	33.3377	58.3377	83.3377
4	31	4.61	-61	28	2.6	1.09718	10.4932	35.4932	60.4932
4	30	28.84	-61	39	32.5	12.7379	20.427	45.427	70.427
4	30	26.85	-61	35	3.1	8.25806	14.1173	39.1173	64.1173
4	31	12.64	-61	27	28.9	2.31846	10.5935	35.5935	60.5935
4	31	8.34	-61	34	13.8	6.25812	12.2653	37.2653	62.2653
4	31	7.7	-61	30	12.1	1.99237	10.5537	35.5537	60.5537
4	31	30.61	-61	38	45	11.9659	19.1603	44.1603	69.1603
4	30	50.84	-61	35	11.7	7.29611	13.1417	38.1417	63.1417
4	30	6.99	-61	35	51.2	10.5581	17.0283	42.0283	67.0283
4	31	39.3	-61	39	51.6	13.5535	21.8335	46.8335	71.8335
4	31	21.54	-61	30	16.3	3.45809	10.8315	35.8315	60.8315
4	31	17.87	-61	35	37.9	8.10492	13.9518	38.9518	63.9518
4	31	42.88	-61	30	20.1	6.12744	12.1684	37.1684	62.1684
4	32	29.88	-61	30	44.6	12.3527	19.7869	44.7869	69.7869
4	31	53.46	-61	29	41.2	7.35707	13.1989	38.1989	63.1989
4	32	4.87	-61	28	49.9	8.81154	14.7464	39.7464	64.7464
4	32	23.53	-61	33	40	12.5615	20.1319	45.1319	70.1319
4	32	58.46	-61	30	5.1	16.044	26.5138	51.5138	76.5138
4	33	22.76	-61	28	45.8	19.2314	33.2211	58.2211	83.2211
4	31	53.72	-61	26	14.4	7.84943	13.6842	38.6842	63.6842
4	31	53.58	-61	27	38.5	7.40951	13.2487	38.2487	63.2487
4	32	57.83	-61	25	47.2	16.2537	26.9321	51.9321	76.9321
4	33	8.58	-61	21	15.4	19.2968	33.366	58.366	83.366
4	32	54.13	-61	21	32.4	17.4229	29.3254	54.3254	79.3254
4	31	53.18	-61	18	50	13.2862	21.3651	46.3651	71.3651
4	31	48.33	-61	16	33.8	15.1859	24.84	49.84	74.84
4	30	56.9	-61	21	47.4	7.81436	13.6483	38.6483	63.6483
4	31	9.75	-61	25	35.8	3.82392	10.9457	35.9457	60.9457
4	30	32.53	-61	12	57.5	18.0609	30.6739	55.6739	80.6739
4	30	39.66	-61	17	51.9	12.481	19.9983	44.9983	69.9983
4	29	5.22	-61	13	21.7	23.0514	42.1282	67.1282	92.1282

Continued

4	29	18.93	-61	14	19.3	21.0332	37.3147	62.3147	87.3147
4	29	36.13	-61	14	50.2	19.1642	33.0723	58.0723	83.0723
4	30	16.68	-61	22	39.4	8.88398	14.8322	39.8322	64.8322
4	29	16.95	-61	19	53.1	16.9168	28.2769	53.2769	78.2769
4	30	12.3	-61	19	46.4	11.8584	18.9892	43.9892	68.9892
4	30	8.45	-61	25	29.8	7.69306	13.5257	38.5257	63.5257
4	31	13.24	-61	27	12.2	2.58166	10.6341	35.6341	60.6341
4	30	0.74	-61	25	54.3	8.43068	14.3083	39.3083	64.3083
4	30	25.99	-61	27	45.9	4.55609	11.2369	36.2369	61.2369
4	30	45.64	-61	35	38.7	7.92215	13.7593	38.7593	63.7593
4	30	58.25	-61	35	36.2	7.67245	13.5051	38.5051	63.5051
4	31	51.9	-61	32	15.1	8.08144	13.9268	38.9268	63.9268
4	31	17.66	-61	27	43.7	2.75006	10.6643	35.6643	60.6643
4	32	52.93	-61	29	36.9	15.2675	24.9967	49.9967	74.9967
4	32	25.62	-61	23	20	13.1002	21.0435	46.0435	71.0435
4	32	48.45	-61	19	47.8	17.7839	30.0849	55.0849	80.0849
4	31	26.94	-61	23	1.3	7.43901	13.2768	38.2768	63.2768
4	32	18.84	-61	19	20.3	15.0363	24.5546	49.5546	74.5546
4	31	48.16	-61	18	2.1	13.7081	22.1077	47.1077	72.1077
4	32	2.49	-61	19	46.6	13.1831	21.1864	46.1864	71.1864
4	32	21.93	-61	10	41.2	23.1181	42.2911	67.2911	92.2911
4	29	33.01	-61	11	24.4	22.6216	41.084	66.084	91.084
4	30	46.27	-61	11	32.2	19.3762	33.5426	58.5426	83.5426
4	30	52.13	-61	10	34.7	20.3955	35.8428	60.8428	85.8428
4	30	18.94	-61	18	6.9	13.0832	21.0142	46.0142	71.0142
4	30	3.77	-61	15	55.4	16.1829	26.7904	51.7904	76.7904
4	30	4.38	-61	22	55.5	9.81363	16.0031	41.0031	66.0031
4	30	55.49	-61	20	14.3	9.55989	15.671	40.671	65.671
4	30	38.92	-61	28	37.5	2.69135	10.6533	35.6533	60.6533
4	29	44.77	-61	30	54.9	10.2157	16.5475	41.5475	66.5475
4	31	0.91	-61	29	57.9	1.37648	10.5055	35.5055	60.5055
4	30	14.72	-61	31	45.4	6.80727	12.7056	37.7056	62.7056
4	30	32.07	-61	42	0.6	15.2798	25.0203	50.0203	75.0203
4	30	56.84	-61	32	2.3	3.68776	10.9008	35.9008	60.9008
4	31	4.72	-61	30	53.4	2.50857	10.622	35.622	60.622
4	31	50.25	-61	30	46.3	7.21385	13.0654	38.0654	63.0654

Table 3. X-ray Data.

Hour	RA			DEC		Count Rate cts·s ⁻¹	Error	Flux ergs·cm ⁻² ·s ⁻¹	Norm
	min	sec	degree	arcmin	arcsec				
4	31	50.03	-61	19	29.7	1.634E-02	1.126E-03	2.257E-13	3.924E-04
4	30	34.31	-61	19	12.6	9.145E-03	8.488E-04	1.264E-13	2.087E-04
4	30	50.16	-61	15	43.9	4.326E-03	5.98E-04	5.977E-14	9.871E-05
4	31	40.34	-61	16	35.3	8.956E-03	8.421E-04	1.237E-13	2.044E-04
4	30	59.59	-61	25	7.2	2.444E-02	1.371E-03	3.377E-13	5.577E-04
4	30	8.03	-61	18	9.3	5.02E-03	6.399E-04	6.936E-14	1.146E-04
4	31	39.39	-61	21	41.8	2.829E-02	1.474E-03	3.909E-13	6.455E-04
4	31	13.2	-61	10	37.9	1.444E-03	3.803E-04	1.995E-14	3.295E-05
4	32	47.12	-61	21	7.2	6.577E-03	7.284E-04	9.083E-14	1.579E-04
4	33	14.12	-61	20	34	1.521E-03	3.878E-04	2.102E-14	3.471E-05
4	32	55.41	-61	19	10.4	3.589E-03	5.531E-04	4.957E-14	8.618E-05
4	32	26.65	-61	21	34.2	1.048E-02	9.079E-04	1.448E-13	2.391E-04
4	30	28.36	-61	17	4	4.716E-03	6.216E-04	6.516E-14	1.076E-04
4	29	44.51	-61	14	56.3	2.154E-03	4.432E-04	2.976E-14	4.915E-05
4	29	57.45	-61	11	45.7	1.97E-03	4.301E-04	2.722E-14	4.495E-05
4	30	56.87	-61	13	33.5	1.945E-03	4.232E-04	2.687E-14	4.438E-05
4	30	58.75	-61	10	21	1.44E-03	3.803E-04	1.99E-14	3.286E-05
4	30	51.24	-61	10	59.7	1.982E-03	4.301E-04	2.739E-14	4.523E-05
4	29	39.59	-61	10	34.5	1.026E-03	3.405E-04	1.418E-14	2.341E-05
4	30	50.35	-61	14	6	2.787E-03	4.924E-04	3.851E-14	6.36E-05
4	29	5.27	-61	13	2.4	1.553E-03	3.953E-04	2.146E-14	3.544E-05
4	30	4.47	-61	23	25.7	7.186E-03	7.554E-04	9.929E-14	1.64E-04
4	30	45.38	-61	23	35.7	1.48E-02	1.071E-03	2.044E-13	3.554E-04
4	29	18.62	-61	19	29.8	1.49E-03	3.802E-04	2.059E-14	3.4E-05
4	29	47.62	-61	23	37	3.907E-03	5.683E-04	5.398E-14	8.915E-05
4	30	22.67	-61	23	19.6	1.448E-02	1.06E-03	2.001E-13	3.304E-04
4	29	24.75	-61	19	5.7	1.342E-03	3.647E-04	1.854E-14	3.062E-05
4	30	53.08	-61	25	14.2	2.126E-02	1.279E-03	2.938E-13	4.851E-04
4	30	28.68	-61	19	39.8	8.539E-03	8.212E-04	1.179E-13	2.05E-04
4	29	32.77	-61	14	52.5	1.329E-03	3.565E-04	1.836E-14	3.033E-05
4	29	27.18	-61	16	51.9	1.778E-03	4.094E-04	2.457E-14	4.057E-05
4	31	8.71	-61	27	7	5.321E-02	2.015E-03	7.349E-13	1.278E-03
4	29	2.33	-61	24	17.2	1.725E-03	4.022E-04	2.383E-14	3.936E-05
4	29	34.78	-61	28	3.7	3.299E-03	5.262E-04	4.558E-14	7.528E-05

Continued

4	29	33.1	-61	15	36.3	2.226E-03	4.497E-04	3.076E-14	5.079E-05
4	30	20.03	-61	26	9.7	1.032E-02	8.982E-04	1.426E-13	2.355E-04
4	29	24.92	-61	26	3.4	2.372E-03	4.558E-04	3.277E-14	5.413E-05
4	29	25.36	-61	33	45.9	1.225E-03	3.484E-04	1.693E-14	2.795E-05
4	30	37.69	-61	29	2.7	1.086E-02	9.204E-04	1.501E-13	2.478E-04
4	30	14.66	-61	28	8.7	9.561E-03	8.656E-04	1.321E-13	2.182E-04
4	30	57	-61	31	7.3	8.431E-03	8.141E-04	1.165E-13	1.924E-04
4	29	48.73	-61	37	32.2	1.226E-03	3.484E-04	1.694E-14	2.798E-05
4	30	52.25	-61	28	13.8	1.883E-02	1.205E-03	2.601E-13	4.521E-04
4	29	8.67	-61	39	6.4	1.77E-03	4.094E-04	2.446E-14	4.039E-05
4	30	32.85	-61	37	55.5	1.785E-03	4.021E-04	2.466E-14	4.073E-05
4	30	45.32	-61	33	0.4	4.251E-03	5.882E-04	5.874E-14	9.7E-05
4	30	39.53	-61	35	7.8	2.569E-03	4.682E-04	3.55E-14	5.862E-05
4	30	18.11	-61	35	8.8	3.167E-03	5.151E-04	4.376E-14	7.227E-05
4	30	37.57	-61	42	49.6	1.35E-03	3.647E-04	1.865E-14	3.081E-05
4	30	59.77	-61	34	38.5	3.789E-03	5.58E-04	5.235E-14	8.646E-05
4	31	31.08	-61	42	8.8	5.201E-04	2.638E-04	7.186E-15	1.187E-05
4	31	17.25	-61	31	49.8	9.111E-03	8.454E-04	1.259E-13	2.079E-04
4	31	42.26	-61	31	39.2	8.115E-03	7.999E-04	1.121E-13	1.852E-04
4	32	13.9	-61	38	12	1.216E-03	3.484E-04	1.68E-14	2.775E-05
4	32	22.39	-61	35	51	1.984E-03	4.231E-04	2.741E-14	4.527E-05
4	32	33.84	-61	38	38.8	1.947E-03	4.232E-04	2.69E-14	4.443E-05
4	32	35.35	-61	29	45.4	5.484E-03	6.663E-04	7.577E-14	1.251E-04
4	32	40.1	-61	25	42.5	1.01E-02	8.919E-04	1.396E-13	2.305E-04
4	31	55.17	-61	30	42	8.868E-03	8.351E-04	1.225E-13	2.129E-04
4	32	45.88	-61	32	56.3	2.804E-03	4.924E-04	3.874E-14	6.398E-05
4	32	42.82	-61	28	11.1	5.853E-03	6.876E-04	8.087E-14	1.336E-04
4	31	23.3	-61	27	26.9	6.611E-02	2.245E-03	9.135E-13	1.509E-03
4	32	47.6	-61	25	11.3	6.143E-03	7.042E-04	8.488E-14	1.402E-04
4	32	13.28	-61	25	40.2	1.97E-02	1.233E-03	2.721E-13	4.73E-04
4	32	41.58	-61	23	3.8	9.254E-03	8.556E-04	1.279E-13	2.112E-04
4	33	9.01	-61	23	12.1	3.671E-03	5.583E-04	5.072E-14	8.377E-05
4	31	37.44	-61	25	52.9	4.432E-02	1.841E-03	6.121E-13	1.064E-03
4	33	16.32	-61	18	0.9	9.65E-04	3.319E-04	1.333E-14	2.202E-05
4	31	14.59	-61	23	44.7	3.37E-02	1.607E-03	4.654E-13	8.092E-04
4	31	21.86	-61	25	17.7	5.875E-02	2.117E-03	8.118E-13	1.341E-03

Continued

4	33	6.66	-61	26	13.7	2.396E-03	4.622E-04	3.309E-14	5.753E-05
4	32	54.18	-61	25	47.7	4.845E-03	6.309E-04	6.691E-14	1.163E-04
4	33	15.31	-61	21	43	2.665E-03	4.866E-04	3.681E-14	6.399E-05
4	31	58.7	-61	16	24.1	6.891E-03	7.44E-04	9.517E-14	1.655E-04
4	32	34.77	-61	14	55.5	2.51E-03	4.747E-04	3.466E-14	6.027E-05
4	32	34.08	-61	13	59.1	1.892E-03	4.234E-04	2.613E-14	4.543E-05
4	30	51.87	-61	23	24.4	1.487E-02	1.074E-03	2.054E-13	3.571E-04
4	32	44.94	-61	16	27	2.439E-03	4.685E-04	3.368E-14	5.856E-05
4	30	41.79	-61	22	43.1	1.35E-02	1.024E-03	1.864E-13	3.242E-04
4	32	12.83	-61	12	32.9	2.123E-03	4.433E-04	2.932E-14	5.098E-05
4	30	43.25	-61	21	6.9	1.266E-02	9.927E-04	1.748E-13	3.04E-04
4	30	54.21	-61	21	3.2	1.501E-02	1.079E-03	2.073E-13	3.604E-04
4	31	8.81	-61	25	10.1	3.408E-02	1.616E-03	4.707E-13	8.183E-04
4	32	0.75	-61	15	3	4.671E-03	6.217E-04	6.451E-14	1.122E-04
4	30	17.05	-61	18	44.1	5.26E-03	6.532E-04	7.264E-14	1.263E-04
4	29	51.03	-61	11	27.3	1.884E-03	4.234E-04	2.602E-14	4.524E-05
4	30	41.88	-61	17	9.9	6.554E-03	7.243E-04	9.051E-14	1.574E-05
4	30	44.89	-61	11	4.6	1.223E-03	3.569E-04	1.689E-14	2.937E-05
4	30	41.86	-61	13	3	2.163E-03	4.432E-04	2.987E-14	5.194E-05
4	29	37.98	-61	14	45.5	1.614E-03	3.951E-04	2.229E-14	3.875E-05
4	29	32.16	-61	13	13	1.587E-03	3.952E-04	2.192E-14	3.811E-05
4	29	26.28	-61	11	55.9	1.26E-03	3.65E-04	1.74E-14	3.025E-05
4	29	2.02	-61	13	54.9	1.559E-03	3.953E-04	2.153E-14	3.743E-05
4	30	7.6	-61	20	3.6	4.963E-03	6.353E-04	6.854E-14	1.192E-04
4	30	33.1	-61	24	22.6	1.586E-02	1.108E-03	2.19E-13	3.808E-04
4	29	7.2	-61	20	18.3	1.708E-03	4.023E-04	2.359E-14	4.101E-05
4	29	12.95	-61	15	8.4	1.058E-03	3.404E-04	1.461E-14	2.54E-05
4	30	59.55	-61	27	40.1	2.718E-02	1.444E-03	3.754E-13	6.526E-04
4	29	51.96	-61	18	12.9	4.704E-03	6.216E-04	6.496E-14	1.13E-04
4	29	27.89	-61	23	37	2.897E-03	4.981E-04	4.001E-14	6.956E-05
4	30	3.09	-61	17	14	4.02E-03	5.784E-04	5.552E-14	9.653E-05
4	30	30.43	-61	20	23.1	1.029E-02	8.983E-04	1.421E-13	2.471E-04
4	30	41.87	-61	27	15.8	1.648E-02	1.128E-03	2.276E-13	3.957E-04
4	29	17.68	-61	28	18.2	2.213E-03	4.43E-04	3.056E-14	5.314E-05
4	30	33.23	-61	33	0.7	4.172E-03	5.833E-04	5.762E-14	1.002E-04
4	29	35.69	-61	31	40.7	2.309E-03	4.494E-04	3.189E-14	5.544E-05

Continued

4	30	21.56	-61	28	48.7	9.564E-03	8.656E-04	1.321E-13	2.296E-04
4	28	47.65	-61	30	52.9	1.025E-03	3.316E-04	1.416E-14	2.461E-05
4	30	53.73	-61	30	5.7	1.048E-02	9.046E-04	1.447E-13	2.516E-04
4	30	26.74	-61	30	31.9	8.654E-03	8.247E-04	1.195E-13	2.078E-04
4	28	56.57	-61	37	53.8	1.535E-03	3.878E-04	2.12E-14	3.686E-05
4	31	4.61	-61	28	2.6	3.796E-02	1.704E-03	5.242E-13	9.115E-04
4	30	28.84	-61	39	32.5	1.995E-03	4.231E-04	2.755E-14	4.79E-05
4	30	26.85	-61	35	3.1	3.02E-03	5.038E-04	4.171E-14	7.252E-05
4	31	12.64	-61	27	28.9	5.944E-02	2.129E-03	8.209E-13	1.427E-03
4	31	8.34	-61	34	13.8	4.474E-03	6.027E-04	6.179E-14	1.074E-04
4	31	7.7	-61	30	12.1	1.268E-02	9.927E-04	1.751E-13	3.045E-04
4	31	30.61	-61	38	45	1.547E-03	3.8E-04	2.136E-14	3.715E-05
4	30	50.84	-61	35	11.7	2.267E-03	4.429E-04	3.131E-14	5.443E-05
4	30	6.99	-61	35	51.2	1.56E-03	3.8E-04	2.154E-14	3.746E-05
4	31	39.3	-61	39	51.6	1.606E-03	3.876E-04	2.218E-14	3.856E-05
4	31	21.54	-61	30	16.3	1.458E-02	1.063E-03	2.014E-13	3.501E-04
4	31	17.87	-61	35	37.9	3.477E-03	5.37E-04	4.802E-14	8.349E-05
4	31	42.88	-61	30	20.1	1.32E-02	1.013E-03	1.823E-13	3.17E-04
4	32	29.88	-61	30	44.6	5.414E-03	6.62E-04	7.477E-14	1.3E-04
4	31	53.46	-61	29	41.2	1.145E-02	9.451E-04	1.581E-13	2.749E-04
4	32	4.87	-61	28	49.9	1.569E-02	1.103E-03	2.168E-13	3.77E-04
4	32	23.53	-61	33	40	2.76E-03	4.86E-04	3.812E-14	6.627E-05
4	32	58.46	-61	30	5.1	2.488E-03	4.684E-04	3.436E-14	5.974E-05
4	33	22.76	-61	28	45.8	1.156E-03	3.487E-04	1.597E-14	2.776E-05
4	31	53.72	-61	26	14.4	2.64E-02	1.424E-03	3.646E-13	6.339E-04
4	31	53.58	-61	27	38.5	3.9E-02	1.728E-03	5.386E-13	9.365E-04
4	32	57.83	-61	25	47.2	4.231E-03	5.932E-04	5.843E-14	1.016E-04
4	33	8.58	-61	21	15.4	4.04E-03	5.835E-04	5.579E-14	9.701E-05
4	32	54.13	-61	21	32.4	5.583E-03	6.75E-04	7.71E-14	1.341E-04
4	31	53.18	-61	18	50	1.466E-02	1.068E-03	2.025E-13	3.52E-04
4	31	48.33	-61	16	33.8	9.482E-03	8.657E-04	1.31E-13	2.277E-04
4	30	56.9	-61	21	47.4	1.312E-02	1.01E-03	1.812E-13	3.15E-04
4	31	9.75	-61	25	35.8	3.568E-02	1.653E-03	4.928E-13	8.567E-04
4	30	32.53	-61	12	57.5	1.931E-03	4.232E-04	2.667E-14	4.637E-05
4	30	39.66	-61	17	51.9	7.007E-03	7.478E-04	9.677E-14	1.682E-04
4	29	5.22	-61	13	21.7	1.253E-03	3.65E-04	1.73E-14	3.009E-05

Continued

4	29	18.93	-61	14	19.3	1.207E-03	3.569E-04	1.667E-14	2.898E-05
4	29	36.13	-61	14	50.2	1.385E-03	3.726E-04	1.913E-14	3.326E-05
4	30	16.68	-61	22	39.4	9.999E-03	8.853E-04	1.381E-13	2.401E-04
4	29	16.95	-61	19	53.1	1.035E-03	3.316E-04	1.429E-14	2.485E-05
4	30	12.3	-61	19	46.4	5.343E-03	6.576E-04	7.379E-14	1.283E-04
4	30	8.45	-61	25	29.8	1.099E-02	9.267E-04	1.518E-13	2.639E-04
4	31	13.24	-61	27	12.2	6.46E-02	2.219E-03	8.922E-13	1.551E-03
4	30	0.74	-61	25	54.3	1.129E-02	9.39E-04	1.559E-13	2.711E-04
4	30	25.99	-61	27	45.9	1.177E-02	9.572E-04	1.626E-13	2.826E-04
4	30	45.64	-61	35	38.7	2.339E-03	4.494E-04	3.23E-14	5.616E-05
4	30	58.25	-61	35	36.2	2.341E-03	4.494E-04	3.233E-14	5.621E-05
4	31	51.9	-61	32	15.1	6.816E-03	7.361E-04	9.413E-14	1.637E-04
4	31	17.66	-61	27	43.7	7.082E-02	2.323E-03	9.781E-13	1.701E-03
4	32	52.93	-61	29	36.9	3.712E-03	5.582E-04	5.126E-14	8.913E-05
4	32	25.62	-61	23	20	1.353E-02	1.027E-03	1.869E-13	3.249E-04
4	32	48.45	-61	19	47.8	4.819E-03	6.309E-04	6.655E-14	1.157E-04
4	31	26.94	-61	23	1.3	3.544E-02	1.647E-03	4.894E-13	8.51E-04
4	32	18.84	-61	19	20.3	9.711E-03	8.756E-04	1.341E-13	2.332E-04
4	31	48.16	-61	18	2.1	1.208E-02	9.722E-04	1.668E-13	2.901E-04
4	32	2.49	-61	19	46.6	1.504E-02	1.082E-03	2.077E-13	3.611E-04
4	32	21.93	-61	10	41.2	1.176E-03	3.57E-04	1.624E-14	2.824E-05
4	29	33.01	-61	11	24.4	1.184E-03	3.57E-04	1.635E-14	2.843E-05
4	30	46.27	-61	11	32.2	1.306E-03	3.648E-04	1.804E-14	3.136E-05
4	30	52.13	-61	10	34.7	1.899E-03	4.233E-04	2.623E-14	4.56E-05
4	30	18.94	-61	18	6.9	5.482E-03	6.663E-04	7.571E-14	1.316E-04
4	30	3.77	-61	15	55.4	3.17E-03	5.208E-04	4.378E-14	7.612E-05
4	30	4.38	-61	22	55.5	6.88E-03	7.4E-04	9.502E-14	1.652E-04
4	30	55.49	-61	20	14.3	1.303E-02	1.007E-03	1.8E-13	3.129E-04
4	30	38.92	-61	28	37.5	1.298E-02	1.004E-03	1.793E-13	3.117E-04
4	29	44.77	-61	30	54.9	2.702E-03	4.804E-04	3.732E-14	6.488E-05
4	31	0.91	-61	29	57.9	1.101E-02	9.266E-04	1.521E-13	2.644E-04
4	30	14.72	-61	31	45.4	1.077E-02	9.173E-04	1.487E-13	2.586E-04
4	30	32.07	-61	42	0.6	1.511E-03	3.801E-04	2.087E-14	3.628E-05
4	30	56.84	-61	32	2.3	6.911E-03	7.4E-04	9.543E-14	1.659E-04
4	31	4.72	-61	30	53.4	8.431E-03	8.141E-04	1.164E-13	2.024E-04
4	31	50.25	-61	30	46.3	9.934E-03	8.821E-04	1.372E-13	2.385E-04

Table 4. Gas Density, Velocity, and Ram Pressure.

hour	RA			DEC		Distance kpc	Ion Density cm ⁻²	Velocity km·s ⁻¹	V _{gal} -V _{cl} km·s ⁻¹	Density g·cm ⁻³	Ram Pressure dyn·cm ⁻²
	min	sec	degree	arcmin	arcsec						
4	31	50.03	-61	19	29.7	572.91	2.7476E-03	15074	-2730	5.9359E-27	4.424E-10
4	30	34.31	-61	19	12.6	700.735	2.073E-03	16872	-932	4.4784E-27	3.8901E-11
4	30	50.16	-61	15	43.9	856.381	1.2916E-03	17054	-750	2.7904E-27	1.5696E-11
4	31	40.34	-61	16	35.3	753.041	1.8544E-03	15604	-2200	4.0062E-27	1.939E-10
4	30	59.59	-61	25	7.2	242.725	3.8631E-03	20962	3158	8.3458E-27	8.3232E-10
4	30	8.03	-61	18	9.3	915.99	1.431E-03	20096	2292	3.0916E-27	1.6241E-10
4	31	39.39	-61	21	41.8	387.482	3.7982E-03	20321	2517	8.2055E-27	5.1985E-10
4	31	13.2	-61	10	37.9	1181.63	6.2505E-04	17929	125	1.3504E-27	2.1099E-13
4	32	47.12	-61	21	7.2	836.301	1.5283E-03	20289	2485	3.3017E-27	2.0389E-10
4	33	14.12	-61	20	34	1067.13	6.4343E-04	18316	512	1.3901E-27	3.644E-12
4	32	55.41	-61	19	10.4	974.164	1.0574E-03	16273	-1531	2.2844E-27	5.3545E-11
4	32	26.65	-61	21	34.2	665.097	2.0346E-03	17959	155	4.3956E-27	1.056E-12
4	30	28.36	-61	17	4	858.674	1.3857E-03	17547	-257	2.9937E-27	1.9773E-12
4	29	44.51	-61	14	56.3	1230	8.1135E-04	17565	-239	1.7528E-27	1.0012E-12
4	29	57.45	-61	11	45.7	1335.45	7.2191E-04	17551	-253	1.5596E-27	9.983E-13
4	30	56.87	-61	13	33.5	991.857	8.0513E-04	16733	-1071	1.7394E-27	1.9952E-11
4	30	58.75	-61	10	21	1219.17	6.1985E-04	17178	-626	1.3391E-27	5.2477E-12
4	30	51.24	-61	10	59.7	1186.98	7.4303E-04	18044	240	1.6052E-27	9.2462E-13
4	29	39.59	-61	10	34.5	1499.66	4.8643E-04	19795	1991	1.0509E-27	4.1658E-11
4	30	50.35	-61	14	6	969.324	9.8085E-04	17101	-703	2.119E-27	1.0473E-11
4	29	5.27	-61	13	2.4	1581.99	5.9283E-04	18756	952	1.2807E-27	1.1607E-11
4	30	4.47	-61	23	25.7	739.598	1.9213E-03	17177	-627	4.1508E-27	1.6318E-11
4	30	45.38	-61	23	35.7	407.641	3.0177E-03	18839	1035	6.5193E-27	6.9837E-11
4	29	18.62	-61	19	29.8	1224.15	7.0553E-04	17425	-379	1.5242E-27	2.1894E-12
4	29	47.62	-61	23	37	877.801	1.3562E-03	16984	-820	2.9299E-27	1.9701E-11
4	30	22.67	-61	23	19.6	593.014	2.8257E-03	18999	1195	6.1047E-27	8.7177E-11
4	29	24.75	-61	19	5.7	1189.19	6.7687E-04	17202	-602	1.4623E-27	5.2995E-12
4	30	53.08	-61	25	14.2	291.649	3.6043E-03	15674	-2130	7.7867E-27	3.5328E-10
4	30	28.68	-61	19	39.8	708.259	2.067E-03	16113	-1691	4.4654E-27	1.2769E-10
4	29	32.77	-61	14	52.5	1309.1	6.1871E-04	17159	-645	1.3367E-27	5.5609E-12
4	29	27.18	-61	16	51.9	1256.94	7.4367E-04	17112	-692	1.6066E-27	7.6935E-12
4	31	8.71	-61	27	7	139.94	5.9017E-03	15025	-2779	1.275E-26	9.8467E-10
4	29	2.33	-61	24	17.2	1259.59	7.7298E-04	15782	-2022	1.67E-27	6.8276E-11
4	29	34.78	-61	28	3.7	966.872	1.2418E-03	18397	593	2.6828E-27	9.4342E-12
4	29	33.1	-61	15	36.3	1271.83	8.1767E-04	17601	-203	1.7665E-27	7.2796E-13

Continued

4	30	20.03	-61	26	9.7	564.658	2.4597E-03	15961	-1843	5.3138E-27	1.8049E-10
4	29	24.92	-61	26	3.4	1049.25	1.0054E-03	17096	-708	2.1721E-27	1.0888E-11
4	29	25.36	-61	33	45.9	1167.06	7.067E-04	17578	-226	1.5268E-27	7.798E-13
4	30	37.69	-61	29	2.7	444.872	2.5933E-03	18504	700	5.6025E-27	2.7452E-11
4	30	14.66	-61	28	8.7	620.558	2.3676E-03	16478	-1326	5.115E-27	8.9936E-11
4	30	57	-61	31	7.3	407.182	2.2869E-03	16743	-1061	4.9407E-27	5.5618E-11
4	29	48.73	-61	37	32.2	1159.08	7.0955E-04	18534	730	1.5329E-27	8.1689E-12
4	30	52.25	-61	28	13.8	303.671	3.5168E-03	15484	-2320	7.5976E-27	4.0893E-10
4	29	8.67	-61	39	6.4	1500.71	7.2863E-04	18136	332	1.5741E-27	1.7351E-12
4	30	32.85	-61	37	55.5	944.776	9.2432E-04	19680	1876	1.9969E-27	7.0278E-11
4	30	45.32	-61	33	0.4	579.626	1.5958E-03	15332	-2472	3.4476E-27	2.1068E-10
4	30	39.53	-61	35	7.8	737.58	1.1947E-03	15664	-2140	2.581E-27	1.182E-10
4	30	18.11	-61	35	8.8	853.185	1.2882E-03	18188	384	2.7831E-27	4.1038E-12
4	30	37.57	-61	42	49.6	1259.53	6.9207E-04	16720	-1084	1.4952E-27	1.7569E-11
4	30	59.77	-61	34	38.5	626.889	1.4766E-03	19966	2162	3.1901E-27	1.4911E-10
4	31	31.08	-61	42	8.8	1143.39	4.3514E-04	16044	-1760	9.4007E-28	2.912E-11
4	31	17.25	-61	31	49.8	387.17	2.356E-03	15790	-2014	5.0899E-27	2.0646E-10
4	31	42.26	-61	31	39.2	402.426	2.1599E-03	16066	-1738	4.6663E-27	1.4095E-10
4	32	13.9	-61	38	12	956.743	6.8673E-04	18262	458	1.4836E-27	3.1121E-12
4	32	22.39	-61	35	51	849.518	9.0024E-04	17605	-199	1.9449E-27	7.7019E-13
4	32	33.84	-61	38	38.8	1074.97	8.1098E-04	19422	1618	1.7521E-27	4.5867E-11
4	32	35.35	-61	29	45.4	667.008	1.5294E-03	19592	1788	3.3041E-27	1.0563E-10
4	32	40.1	-61	25	42.5	672.069	2.0146E-03	16942	-862	4.3524E-27	3.234E-11
4	31	55.17	-61	30	42	405.088	2.2672E-03	17380	-424	4.8981E-27	8.8056E-12
4	32	45.88	-61	32	56.3	854.96	1.0279E-03	17385	-419	2.2207E-27	3.8987E-12
4	32	42.82	-61	28	11.1	701.442	1.5363E-03	18314	510	3.319E-27	8.6326E-12
4	31	23.3	-61	27	26.9	60.3938	6.3767E-03	17841	37	1.3776E-26	1.886E-13
4	32	47.6	-61	25	11.3	742.353	1.5193E-03	17305	-499	3.2823E-27	8.1728E-12
4	32	13.28	-61	25	40.2	438.438	3.1762E-03	16389	-1415	6.8619E-27	1.3739E-10
4	32	41.58	-61	23	3.8	730.969	1.8607E-03	17301	-503	4.0199E-27	1.0171E-11
4	33	9.01	-61	23	12.1	957.477	1.0573E-03	16301	-1503	2.2841E-27	5.1598E-11
4	31	37.44	-61	25	52.9	129.74	5.221E-03	15324	-2480	1.1279E-26	6.9373E-10
4	33	16.32	-61	18	0.9	1175.16	4.8635E-04	17084	-720	1.0507E-27	5.4469E-12
4	31	14.59	-61	23	44.7	228.465	4.5582E-03	19346	1542	9.8475E-27	2.3415E-10
4	31	21.86	-61	25	17.7	100.452	5.9436E-03	18944	1140	1.2841E-26	1.6688E-10
4	33	6.66	-61	26	13.7	902.641	9.0863E-04	17843	39	1.963E-27	2.9857E-14
4	32	54.18	-61	25	47.7	794.861	1.3549E-03	15211	-2593	2.9272E-27	1.9681E-10

Continued

4	33	15.31	-61	21	43	1044.12	8.8472E-04	18418	614	1.9114E-27	7.2057E-12
4	31	58.7	-61	16	24.1	812.513	1.6052E-03	18574	770	3.4679E-27	2.0561E-11
4	32	34.77	-61	14	55.5	1063.63	8.5224E-04	18999	1195	1.8412E-27	2.6293E-11
4	32	34.08	-61	13	59.1	1117.12	7.226E-04	17160	-644	1.5611E-27	6.4744E-12
4	30	51.87	-61	23	24.4	369.989	3.0246E-03	17179	-625	6.5344E-27	2.5525E-11
4	32	44.94	-61	16	27	1034.41	8.4873E-04	20443	2639	1.8336E-27	1.277E-10
4	30	41.79	-61	22	43.1	470.951	2.8328E-03	16815	-989	6.1199E-27	5.986E-11
4	32	12.83	-61	12	32.9	1122.36	7.7045E-04	17884	80	1.6645E-27	1.0653E-13
4	30	43.25	-61	21	6.9	542.605	2.6529E-03	18739	935	5.7314E-27	5.0105E-11
4	30	54.21	-61	21	3.2	487.828	2.8999E-03	18554	750	6.2629E-27	3.5229E-11
4	31	8.81	-61	25	10.1	172.409	4.6737E-03	19241	1437	1.0097E-26	2.085E-10
4	32	0.75	-61	15	3	911.775	1.2637E-03	17017	-787	2.73E-27	1.6909E-11
4	30	17.05	-61	18	44.1	828.953	1.553E-03	16940	-864	3.3552E-27	2.5046E-11
4	29	51.03	-61	11	27.3	1386.88	7.0946E-04	17729	-75	1.5327E-27	8.6216E-14
4	30	41.88	-61	17	9.9	790.061	1.7026E-03	16800	-1004	3.6783E-27	3.7078E-11
4	30	44.89	-61	11	4.6	1196.17	5.9927E-04	17619	-185	1.2947E-27	4.431E-13
4	30	41.86	-61	13	3	1066.98	8.519E-04	17094	-710	1.8405E-27	9.2777E-12
4	29	37.98	-61	14	45.5	1280.83	7.0591E-04	18316	512	1.5251E-27	3.9979E-12
4	29	32.16	-61	13	13	1396.9	6.607E-04	16861	-943	1.4274E-27	1.2693E-11
4	29	26.28	-61	11	55.9	1501.01	5.5977E-04	19447	1643	1.2093E-27	3.2645E-11
4	29	2.02	-61	13	54.9	1564.73	6.1738E-04	17650	-154	1.3338E-27	3.1632E-13
4	30	7.6	-61	20	3.6	829.675	1.5355E-03	16615	-1189	3.3172E-27	4.6897E-11
4	30	33.1	-61	24	22.6	478.578	3.126E-03	16253	-1551	6.7535E-27	1.6246E-10
4	29	7.2	-61	20	18.3	1292.92	7.5746E-04	18086	282	1.6364E-27	1.3014E-12
4	29	12.95	-61	15	8.4	1433.28	5.4089E-04	19138	1334	1.1685E-27	2.0795E-11
4	30	59.55	-61	27	40.1	228.912	4.2247E-03	16020	-1784	9.1271E-27	2.9049E-10
4	29	51.96	-61	18	12.9	1021.56	1.3736E-03	16924	-880	2.9674E-27	2.298E-11
4	29	27.89	-61	23	37	1046.75	1.1219E-03	19230	1426	2.4237E-27	4.9286E-11
4	30	3.09	-61	17	14	994.406	1.2662E-03	19803	1999	2.7354E-27	1.0931E-10
4	30	30.43	-61	20	23.1	659.584	2.3187E-03	17422	-382	5.0093E-27	7.3098E-12
4	30	41.87	-61	27	15.8	374.249	3.2775E-03	18851	1047	7.0806E-27	7.7618E-11
4	29	17.68	-61	28	18.2	1118.19	9.7861E-04	16611	-1193	2.1142E-27	3.009E-11
4	30	33.23	-61	33	0.7	647.975	1.6065E-03	19579	1775	3.4706E-27	1.0935E-10
4	29	35.69	-61	31	40.7	1022.05	1.0567E-03	19537	1733	2.283E-27	6.8565E-11
4	30	21.56	-61	28	48.7	572.642	2.4576E-03	19556	1752	5.3094E-27	1.6297E-10
4	28	47.65	-61	30	52.9	1409.58	5.8696E-04	16577	-1227	1.2681E-27	1.9091E-11
4	30	53.73	-61	30	5.7	368.955	2.6218E-03	19566	1762	5.6642E-27	1.7585E-10

Continued

4	30	26.74	-61	30	31.9	579.922	2.3443E-03	17322	-482	5.0646E-27	1.1766E-11
4	28	56.57	-61	37	53.8	1536.47	6.8442E-04	16438	-1366	1.4786E-27	2.7591E-11
4	31	4.61	-61	28	2.6	200.33	4.9934E-03	18436	632	1.0788E-26	4.3089E-11
4	30	28.84	-61	39	32.5	1066.38	9.5169E-04	18443	639	2.056E-27	8.3952E-12
4	30	26.85	-61	35	3.1	797.672	1.3116E-03	18954	1150	2.8335E-27	3.7473E-11
4	31	12.64	-61	27	28.9	118.546	6.2351E-03	17815	11	1.347E-26	1.6299E-14
4	31	8.34	-61	34	13.8	575.962	1.6543E-03	16828	-976	3.5739E-27	3.4044E-11
4	31	7.7	-61	30	12.1	299.563	2.8826E-03	19017	1213	6.2275E-27	9.1629E-11
4	31	30.61	-61	38	45	893.592	8.5656E-04	19018	1214	1.8505E-27	2.7273E-11
4	30	50.84	-61	35	11.7	694.436	1.1577E-03	19051	1247	2.5011E-27	3.8893E-11
4	30	6.99	-61	35	51.2	958.211	8.9319E-04	17831	27	1.9297E-27	1.4067E-14
4	31	39.3	-61	39	51.6	982.534	8.3394E-04	17263	-541	1.8016E-27	5.2731E-12
4	31	21.54	-61	30	16.3	268.719	3.0735E-03	16782	-1022	6.64E-27	6.9353E-11
4	31	17.87	-61	35	37.9	664.515	1.4117E-03	20052	2248	3.0498E-27	1.5412E-10
4	31	42.88	-61	30	20.1	318.514	2.8475E-03	18340	536	6.1518E-27	1.7674E-11
4	32	29.88	-61	30	44.6	652.299	1.5851E-03	16247	-1557	3.4244E-27	8.3016E-11
4	31	53.46	-61	29	41.2	342.161	2.5989E-03	18611	807	5.6146E-27	3.6565E-11
4	32	4.87	-61	28	49.9	393.206	2.955E-03	18754	950	6.3841E-27	5.7616E-11
4	32	23.53	-61	33	40	734.949	1.1251E-03	17724	-80	2.4306E-27	1.5556E-13
4	32	58.46	-61	30	5.1	867.206	9.631E-04	17327	-477	2.0807E-27	4.7341E-12
4	33	22.76	-61	28	45.8	1054.78	5.9493E-04	18867	1063	1.2853E-27	1.4523E-11
4	31	53.72	-61	26	14.4	262.149	3.9098E-03	17975	171	8.4467E-27	2.4699E-12
4	31	53.58	-61	27	38.5	269.631	4.7922E-03	17485	-319	1.0353E-26	1.0535E-11
4	32	57.83	-61	25	47.2	826.926	1.2479E-03	17649	-155	2.696E-27	6.4772E-13
4	33	8.58	-61	21	15.4	1001.73	1.1099E-03	17968	164	2.3978E-27	6.4492E-13
4	32	54.13	-61	21	32.4	877.067	1.383E-03	16675	-1129	2.9877E-27	3.8083E-11
4	31	53.18	-61	18	50	628.685	2.5394E-03	17516	-288	5.4861E-27	4.5504E-12
4	31	48.33	-61	16	33.8	771.326	1.9301E-03	20996	3192	4.1698E-27	4.2485E-10
4	30	56.9	-61	21	47.4	429.472	2.758E-03	17310	-494	5.9584E-27	1.4541E-11
4	31	9.75	-61	25	35.8	147.512	4.7968E-03	18530	726	1.0363E-26	5.462E-11
4	30	32.53	-61	12	57.5	1104.62	7.9732E-04	15292	-2512	1.7225E-27	1.087E-10
4	30	39.66	-61	17	51.9	754.95	1.7965E-03	17315	-489	3.8811E-27	9.2805E-12
4	29	5.22	-61	13	21.7	1567.39	5.5071E-04	16185	-1619	1.1898E-27	3.1185E-11
4	29	18.93	-61	14	19.3	1428.65	5.7492E-04	16192	-1612	1.2421E-27	3.2275E-11
4	29	36.13	-61	14	50.2	1288.91	6.5256E-04	17003	-801	1.4098E-27	9.0453E-12
4	30	16.68	-61	22	39.4	661.843	2.3545E-03	18279	475	5.0866E-27	1.1477E-11
4	29	16.95	-61	19	53.1	1225.5	6.0471E-04	18302	498	1.3064E-27	3.24E-12

Continued

4	30	12.3	-61	19	46.4	809.427	1.5966E-03	18852	1048	3.4492E-27	3.7883E-11
4	30	8.45	-61	25	29.8	670.808	2.5304E-03	16346	-1458	5.4666E-27	1.1621E-10
4	31	13.24	-61	27	12.2	104.311	6.495E-03	18343	539	1.4032E-26	4.0765E-11
4	30	0.74	-61	25	54.3	735.28	2.5267E-03	17973	169	5.4586E-27	1.559E-12
4	30	25.99	-61	27	45.9	517.688	2.7389E-03	17443	-361	5.9171E-27	7.7112E-12
4	30	45.64	-61	35	38.7	744.156	1.1621E-03	18143	339	2.5105E-27	2.8851E-12
4	30	58.25	-61	35	36.2	698.054	1.1683E-03	18741	937	2.5239E-27	2.2159E-11
4	31	51.9	-61	32	15.1	480.197	1.9777E-03	18967	1163	4.2726E-27	5.7789E-11
4	31	17.66	-61	27	43.7	98.4949	6.7977E-03	18931	1127	1.4686E-26	1.8653E-10
4	32	52.93	-61	29	36.9	810.925	1.2046E-03	17893	89	2.6024E-27	2.0613E-13
4	32	25.62	-61	23	20	593.535	2.4529E-03	17121	-683	5.2992E-27	2.472E-11
4	32	48.45	-61	19	47.8	897.545	1.2703E-03	18819	1015	2.7444E-27	2.8273E-11
4	31	26.94	-61	23	1.3	266.986	4.5657E-03	15589	-2215	9.8638E-27	4.8394E-10
4	32	18.84	-61	19	20.3	721.781	1.9621E-03	17349	-455	4.239E-27	8.7757E-12
4	31	48.16	-61	18	2.1	667.423	2.277E-03	17878	74	4.9193E-27	2.6938E-13
4	32	2.49	-61	19	46.6	607.527	2.5797E-03	15928	-1876	5.5732E-27	1.9614E-10
4	32	21.93	-61	10	41.2	1279.99	5.3243E-04	19706	1902	1.1503E+27	4.1612E-11
4	29	33.01	-61	11	24.4	1489.4	5.4236E-04	16971	-833	1.1717E-27	8.1304E-12
4	30	46.27	-61	11	32.2	1160.23	6.295E-04	16057	-1747	1.36E-27	4.1506E-11
4	30	52.13	-61	10	34.7	1214.9	7.3551E-04	17785	-19	1.589E-27	5.7363E-15
4	30	18.94	-61	18	6.9	850.29	1.5619E-03	19080	1276	3.3743E-27	5.4939E-11
4	30	3.77	-61	15	55.4	1059.89	1.0825E-03	18261	457	2.3387E-27	4.8843E-12
4	30	4.38	-61	22	55.5	753.058	1.911E-03	17431	-373	4.1286E-27	5.744E-12
4	30	55.49	-61	20	14.3	533.91	2.6462E-03	16672	-1132	5.7168E-27	7.3256E-11
4	30	38.92	-61	28	37.5	423.35	2.9105E-03	20213	2409	6.2879E-27	3.6491E-10
4	29	44.77	-61	30	54.9	927.796	1.1858E-03	16408	-1396	2.5617E-27	4.9923E-11
4	31	0.91	-61	29	57.9	318.831	2.6887E-03	20087	2283	5.8087E-27	3.0275E-10
4	30	14.72	-61	31	45.4	716.612	2.5449E-03	17011	-793	5.4981E-27	3.4574E-11
4	30	32.07	-61	42	0.6	1220.01	7.6823E-04	16941	-863	1.6597E-27	1.2361E-11
4	30	56.84	-61	32	2.3	464.289	2.1128E-03	19685	1881	4.5644E-27	1.615E-10
4	31	4.72	-61	30	53.4	356.561	2.3469E-03	19538	1734	5.0701E-27	1.5245E-10
4	31	50.25	-61	30	46.3	381.508	2.427E-03	17140	-664	5.2432E-27	2.3117E-11

brightness, as can be seen in [Figure 2](#). That is why a simple radial analysis, which assumes azimuthal symmetry is insufficient, justifying the analysis here that uses local density, to reflect gas distribution asymmetries from the merger.

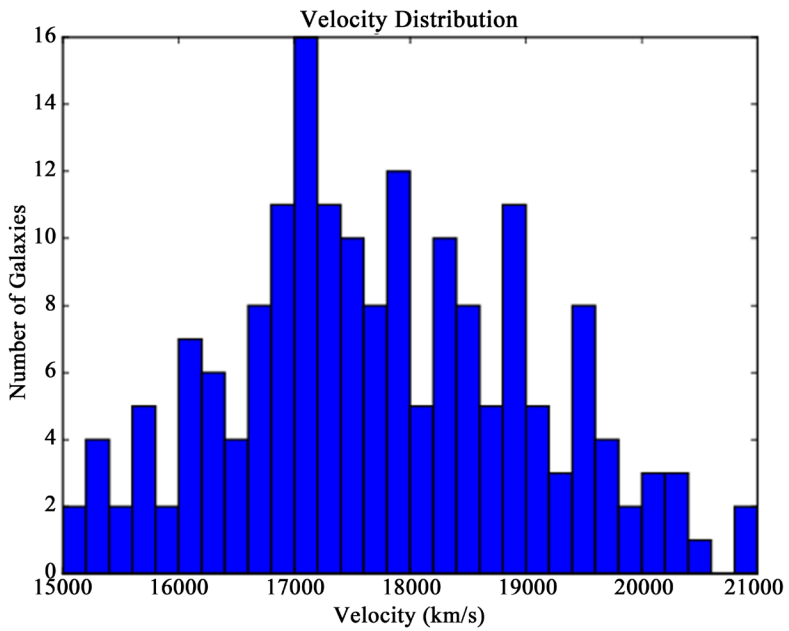


Figure 1. Histogram of the galaxy velocities. The zero point is the velocity of the cluster, 17,804 km·s⁻¹, $z = 0.0594$. The bin width is 200 km·s⁻¹. Significant asymmetry is visible due to the merger.

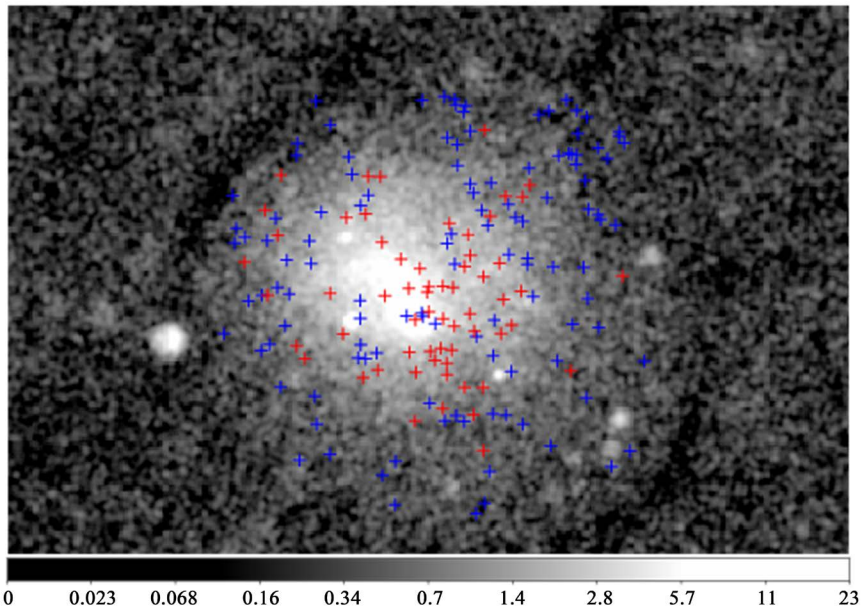


Figure 2. Positions of galaxies overlaid on the x-ray image of Abell 3266 color coded to show ram pressure strength. Red depicts a galaxy with ram pressure $> 5 \times 10^{-11} \text{ dyn}\cdot\text{cm}^{-2}$ and blue a galaxy with ram pressure $\leq 5 \times 10^{-11} \text{ dyn}\cdot\text{cm}^{-2}$.

4. Results

The ram pressure for each galaxy, ρv^2 , was calculated using the gas densities and velocities in **Table 4**. **Figure 3** shows the histogram of ram pressure for the 177 galaxies in this study. As can be seen by observing the histogram, the galaxies experience a large range of ram pressure. We adopted the condition for high ram

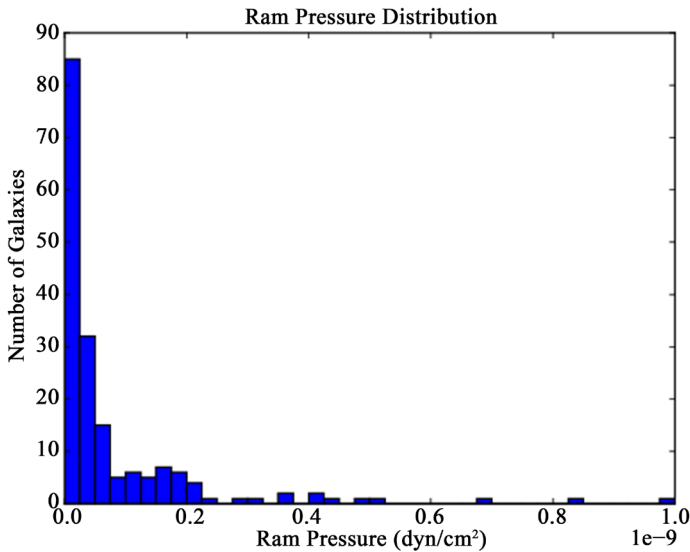


Figure 3. Histogram of the ram pressure for each galaxy. The first two bins contain all galaxies with low ram pressure.

pressure used by [50] of 5×10^{-11} dynes \cdot cm $^{-2}$. Of the 177 galaxies used, 61 galaxies were found to have ram pressures that can be considered “high” (*i.e.* $\geq 5 \times 10^{-11}$ dyn \cdot cm $^{-2}$). The remaining 116 galaxies were found to have “low” ram pressures. The calculated ram pressures for each of the 177 galaxies are listed in **Table 4**. We would expect to see galaxies with high ram pressures in regions where the density is high, or in galaxies with high velocities with respect to the cluster. In **Figure 2**, the distribution of these galaxies can be seen overlaid on the x-ray image of the cluster. Galaxies with low and high ram pressure appear throughout the cluster though high ram pressure galaxies tend to be closer to the center.

Star formation in galaxies is enhanced by the ram pressure they experience. This is seen in both simulations and observations. To assess whether a galaxy is currently experiencing or recently experienced an enhancement in star formation, we inspected the equivalent width of H β and [OII] for each galaxy in the study. **Figure 4** and **Figure 5** show the histogram of equivalent width of H β and [OII], respectively.

It is believed that the surrounding environment can impact how the galaxy evolves (e.g. [17] [51] [52] [53] [54]). If there is a correlation between ram pressure and star formation in Abell 3266, it should be apparent when comparing a histogram of equivalent widths for galaxies with high ram pressures versus galaxies with low ram pressures. **Figure 6** and **Figure 7** show the histograms of the equivalent width of H β and [OII], respectively, plotted based on whether the galaxy has high or low ram pressure. Note that if the equivalent width of H β is positive (negative), this corresponds to absorption (emission). Perhaps there is a weak correlation that is buried in the large, inclusive samples.

To evaluate this hypothesis, we addressed the fact that the equivalent widths of H β and [OII] obtained from WINGS do not all have a signal to noise of 3σ or greater. For this reason we have created two subsamples which will be referred to

as Sample A and Sample B. Sample A consists of all galaxies with line emission greater than 3σ significance. Sample A consists of a total of 34 galaxies for H β and 24 for O[II]. [Figure 8](#) and [Figure 9](#) show a plot of O[II] verses ram pressure and H β verses ram pressure, respectively, for the Sample A galaxies. Sample B is a subgroup of Sample A, consisting of all galaxies with a signal to noise greater than 3σ for both H β and [OII]. Sample B consists of a total of 12 galaxies. [Figure 10](#) and [Figure 11](#) show a plot of H β verses ram pressure and [OII] verses ram pressure, respectively for Sample B galaxies. Sample B is the highest quality sub-sample. However, in all of the data samples, there is no apparent correlation between H β or O[II] line strength and ram-pressure.

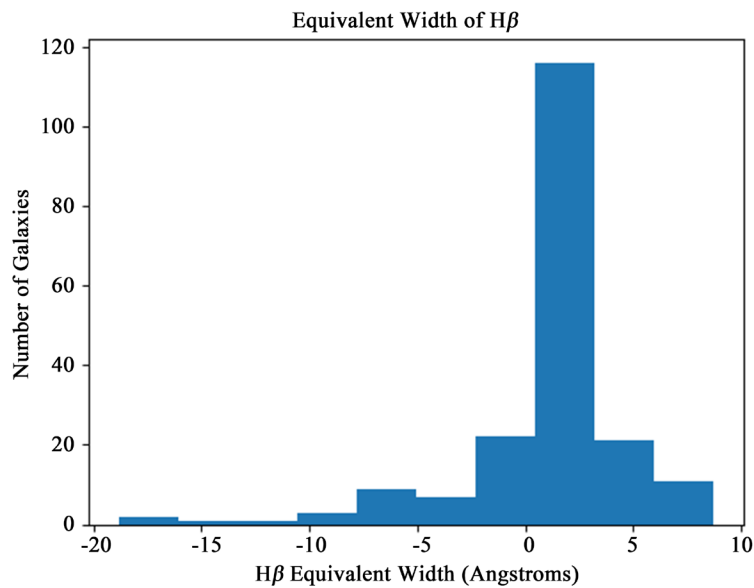


[Figure 4.](#) Histogram of the equivalent width of H β . Each bin has a width of 0.5 Å.

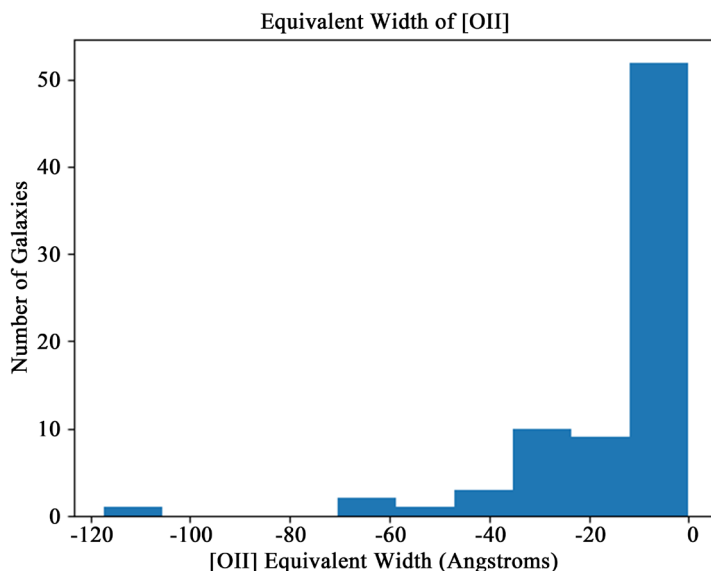


[Figure 5.](#) Histogram of the equivalent width of [OII] emission lines. Each bin has a width of 2.5 Å.

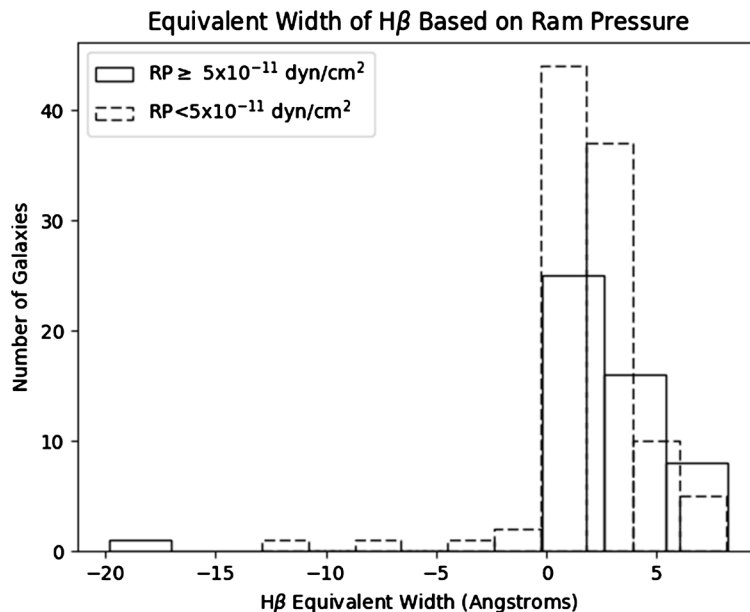


Figure 6. Histogram of H β equivalent width based on the ram pressure of the galaxy. The solid histogram corresponds to high ram pressure ($\geq 5 \times 10^{-11}$ dyn·cm $^{-2}$). The black dashed histogram corresponds to low ram pressure ($< 5 \times 10^{-11}$ dyn·cm $^{-2}$). Each bin has a width of 0.5 Å. The low and high ram pressure galaxies span the same range of absorption line strength though the high absorption line galaxies have a higher fraction of high ram pressure galaxies. Low absorption line galaxies are preferentially low ram pressure.

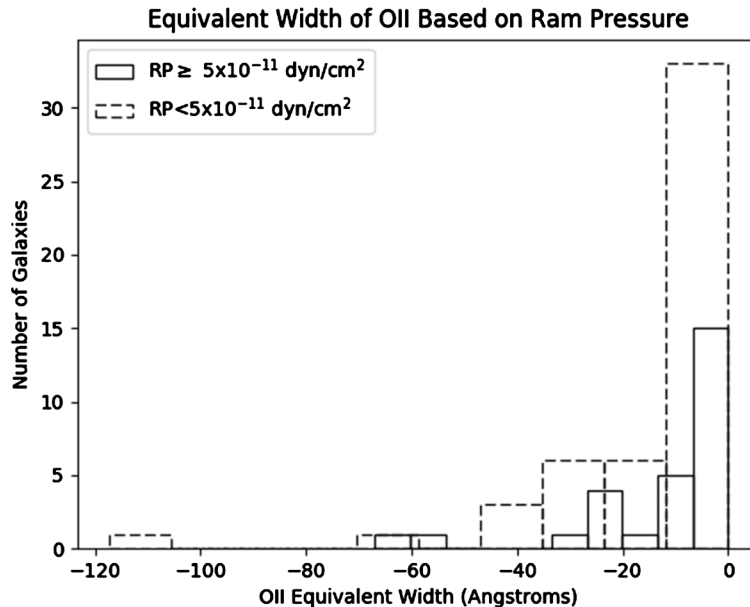


Figure 7. Histogram of [OII] equivalent width based on the ram pressure of the galaxy. The solid histogram corresponds to high ram pressure ($\geq 5 \times 10^{-11}$ dyn·cm $^{-2}$). The black dashed histogram corresponds to low ram pressure ($< 5 \times 10^{-11}$ dyn·cm $^{-2}$). Each bin has a width of 2.5 Å.

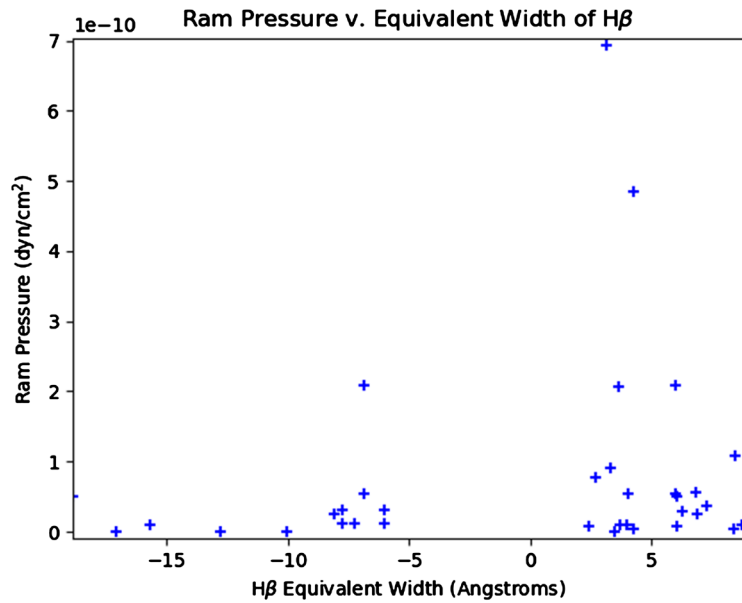


Figure 8. Plot of equivalent width of [OII] verses ram pressure for Sample A.

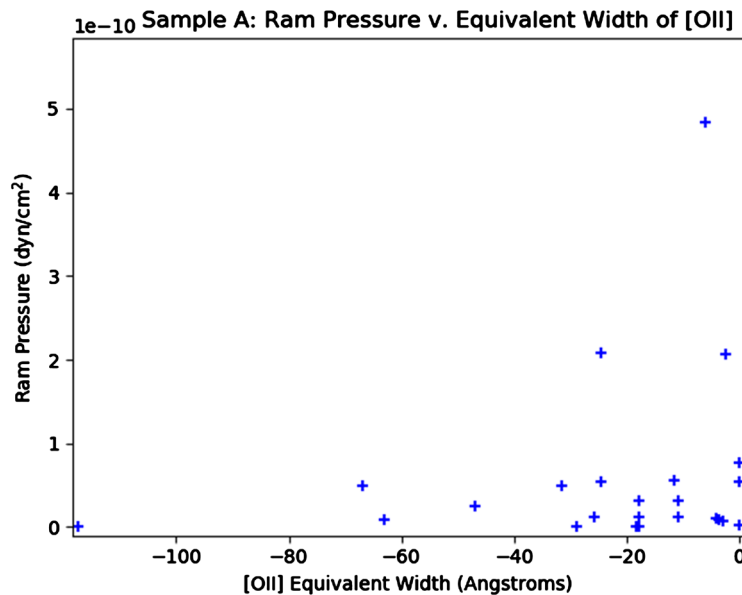


Figure 9. Plot of equivalent width of H β verses ram pressure for sample A, the 34 galaxies with 3 sigma significance. There is no visible preference for galaxies with H β in emission to be in a region of high ram pressure.

E + A Galaxies

[54] defines an E + A galaxy as one with Balmer absorptions lines that are $(H\delta + H\gamma + H\beta)/3 \geq 4\text{\AA}$, and [OII] emission lines are $< 5\text{\AA}$. For our criteria, we come as close as we can to this with our database by requiring an equivalent width of either H β or H $\delta > 4\text{\AA}$, and equivalent width of [OII] $< -5\text{\AA}$. There are 6 galaxies out of the 71 (that have spectroscopic coverage) or 8.5% that meet these classification requirements. Of those 6, 3 have “high” ram pressures $> 5 \times 10^{-11}$, while the other 3 have “low” ram pressures. Therefore, the data do not support a

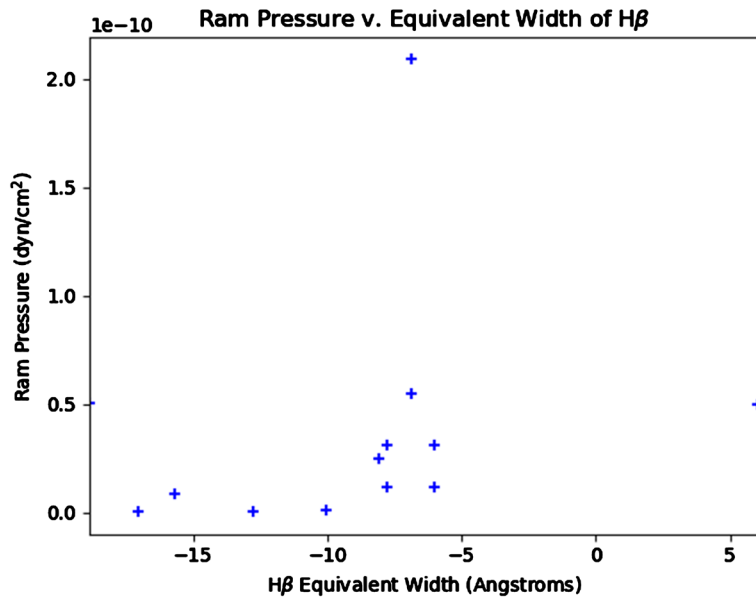


Figure 10. Log-log plot of the equivalent width of H β verses ram pressure for the 12 galaxies (Sample B) with both H β and O[II] lines of higher than 3σ significance.

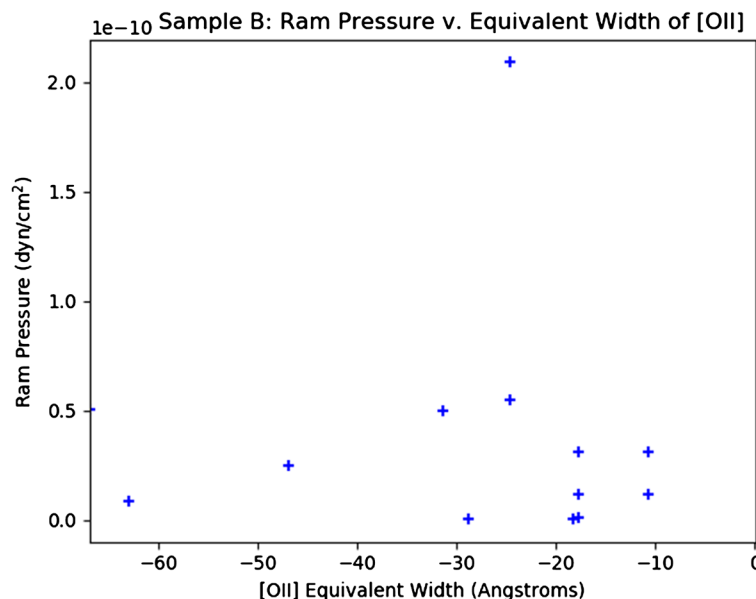


Figure 11. Log-log plot of the equivalent width of O[II] verses ram pressure for 12 galaxies with both H β and O[II] lines of higher than 3σ significance.

correlation between the E + A phenomenon and ram pressure. However, the frequency of E + A galaxies, 8.5% is substantially higher than the fraction found in a non-merging cluster, Coma [55] and this indicates a galaxy evolutionary effect associated with the merger.

5. Discussion

The relationship between ram pressure and star formation during a cluster merger was investigated for Abell 3266. This galaxy cluster was chosen because it

shows evidence of a merger in progress: very high velocity dispersion in the center, an asymmetric density distribution, and regions of shock heated gas. Thus, it is the best opportunity to catch an increase in star formation due to RPS before the galaxies are quenched. Spectral type O and B type stars emit continuum radiation that ionizes Hydrogen in the surrounding medium. The Hydrogen ions then recombine with free electrons producing recombination emission lines. These emission lines are believed to correspond to HII regions surrounding O and B type stars. Other stellar classes, such as A and F type stars, do not produce strong enough radiation to ionize the surrounding gas and thus are lacking Hydrogen emission lines. Because of the short lifetime of the high mass stars, this emission line should track starburst galaxies. We found that the galaxies exhibiting H β in emission do not correlate with high ram pressure in our study. We do not see evidence of a widespread RPS induced starburst phase associated with the merger. There may be evidence of an increased level of recent star formation due to the merger, but we don't find a direct link to ram pressure. We then turn our attention to the possibility of post-starburst galaxies and their correlation with ram pressure.

An episode of rapid star formation would consume a large percentage of the gas available in the galaxy. This consumption, coupled with ram pressure stripping, would lead to a termination of star formation. While the brief timescale of enhanced star formation via RPS is critical to whether or not a correlation is observed it is possible to detect the post-starburst galaxies as E + A galaxies. An E + A galaxy has a characteristic spectrum, displaying strong Balmer absorption and little or no [OII] emission ([44] [55] [56]). The star formation observed in an E + A galaxy is understood to have occurred within the last 1.5 Gyr [57]. [56] observed that the number of E + A galaxies found in intermediate redshift clusters is greater than the number found in the field. This implies that environment is important in their formation. Such events as ram pressure stripping could play a role in the increased number of post starburst galaxies found in clusters versus the field. [56] and [58] both observe that E + A's are generally located outside of the cluster core, which may be a result of their continued motion after RPS induced starburst.

The [OII] emission comes from the medium surrounding hot, young stars, namely O and B type stars. The optimum conditions for producing [OII] emission can be found in HII regions [46]. This makes the [OII] emission line a good indication of young stellar populations. If the [OII] emission line is very weak, or absent, it is likely that there is no current star formation occurring in the galaxy. Pairing this information with strong Balmer absorption lines allows us to classify galaxies as post starburst. If there was a recent starburst in a galaxy, there will still be some O and B type stars present which have not reached the end of their lifetime (1 - 10 Myr); however, there will be very little gas remaining in the former HII regions, resulting in a lack of [OII] emission. The A and F type stars, with lifetimes on the order of 1 Gyr or longer, will still provide strong Balmer

absorption lines in the spectra of those galaxies. We find here that 8.5% or 6 out of 71 of the galaxies that have both OII and H β or H δ available are E + A galaxies. [56] find E + A's make up a non-negligible component of the cluster population (7% - 13%) at intermediate redshifts. These authors point out that compared to the low E + A fraction in Coma (3%) [55] their results show the E + A fraction evolves strongly with redshift. We find a comparable fraction, 8.5% in Abell 3266, a low redshift merging cluster to the intermediate redshift clusters. Within our limited sample we can say the E + A fraction is higher in this merging cluster compared to the nearby Coma cluster. The 6 E + A galaxies are split evenly between high and low ram pressure. While this E + A analysis does not show a correlation between post starburst galaxies and high ram pressure, the lack of immediacy in this phenomena means that it is likely the E + A galaxies are observed in a different gas environment than the one they were formed in.

The lack of a strong global correlation between ram-pressure and optical star formation indicators may also be complicated by the multiplicity of cluster environmental effects on galaxy evolution. For example, radio observations reveal an asymmetric, truncated distribution of HI in the spiral galaxy, UGC 07049, in the NGC 4065 group of galaxies [59]. In addition, radio continuum emission reveals strong star formation in the galaxy. The authors conclude that a combination of tidal and ram-pressure stripping is most likely necessary to produce the HI deficiency and disk asymmetry. In a study of three Virgo Cluster galaxies, in one of the galaxies, NGC 4264, X-ray observations at the position of magnetic field enhancements do not show compressional heating as expected from a strong adiabatic shock due to ram pressure. This favors tidal interactions rather than ram pressure stripping. Conversely, NGC 4569's radio polarized ridge shows a higher temperature, indicative of ram-pressure shocked gas. The third galaxy, NGC 2276, shows no clear indications of a shock, which is consistent with the observed distortions coming from tidal interaction [60].

Finally, though there is evidence of an ongoing merger in Abell 3266, it may have previously had a major merger at an earlier epoch that resulted in cluster wide quenching of star formation diminishing the effect of the present merger. Support for this idea comes from studies at intermediate redshift. [61] finds that star formation takes place throughout the stellar disk in $0.3 < z < 0.6$ galaxies though cluster galaxies have a significantly smaller H α disk than field galaxies. The authors concluded that ram-pressure stripping and disk strangulation can account for this result. The high level of E + A galaxies we find is consistent with a larger merger within the last billion years.

6. Conclusion

Through this work, the properties of ram pressure and H β equivalent width are examined for 177 galaxies located in the merging galaxy cluster Abell 3266. There are cases of ram pressure induced star formation within galaxies, the so called Jellyfish galaxies that appear to be associated with cluster merger. Al-

though Abell 3266 is an ongoing merger the expected relationship between ram pressure and H β equivalent width was not observed. This shows a lack of evidence for ongoing global star formation due to ram pressure at this point of the merger. To test whether star formation had recently ended, we identified galaxies whose spectra were characteristic of E + A galaxies, or post starburst galaxies. There did not appear to be a correlation with E + A galaxies and ram pressure either. However, there is an enhancement in the number of E + A galaxies in this merging cluster compared to a quiescent cluster or the field, which is consistent with a major merger in the past billion years. The evidence contained in this work does not provide clear support that star formation is currently enhanced globally by ram pressure globally. But because simulations show that the enhanced star formation phase is short and depends sensitively on the environment conditions the galaxy encounters, we conclude that this phase is episodic, involving only a small fraction of the cluster galaxies at any epoch. The lack of correlation is also likely the result of the galaxy's continued motion after the RPS induced star formation phase.

Conflicts of Interest

The authors declare no conflicts of interest regarding the publication of this paper.

References

- [1] Bahcall, N. (1988) Large-Scale Structure in the Universe Indicated by Galaxy Clusters. *Annual Reviews of Astronomy and Astrophysics*, **26**, 631.
<https://doi.org/10.1146/annurev.aa.26.090188.003215>
- [2] Jimnez-Teja, Y., *et al.* (2019) J-PLUS: Analysis of the Intracluster Light in the Coma Cluster. *Astronomy and Astrophysics*, **622**, A183.
<https://doi.org/10.1051/0004-6361/201833547>
- [3] de Plaa, *et al.* (2007) Constraining Supernova Models Using the Hot Gas in Clusters of Galaxies. *Astronomy and Astrophysics*, **465**, 34.
<https://doi.org/10.1051/0004-6361:20066382>
- [4] Simionescu, A., *et al.* (2009) Chemical Enrichment in the Cluster of Galaxies Hydra A. *Astronomy and Astrophysics*, **493**, 409.
<https://doi.org/10.1051/0004-6361:200810225>
- [5] Medvedev, P., *et al.* (2014) Impact of Thermal Diffusion and Other Abundance Anomalies on Cosmological Uses of Galaxy Clusters. *Monthly Notices of the Royal Astronomical Society*, **440**, 2464. <https://doi.org/10.1093/mnras/stu434>
- [6] Sarazin, C.-L. (1988) X-Ray Emission from Clusters of Galaxies. Cambridge University Press, Cambridge.
- [7] Gunn, J.E. and Gott, J.R. III (1972) On the Infall of Matter into Clusters of Galaxies and Some Effects on Their Evolution. *Astrophysical Journal*, **176**, 1-19.
<https://doi.org/10.1086/151605>
- [8] Smith, R.-J., Lucey, J.-R., Hammer, D., *et al.* (2010) Ultraviolet Tails and Trails in Cluster Galaxies: A Sample of Candidate Gaseous Stripping Events in Coma. *Monthly Notices of the Royal Astronomical Society*, **408**, 1417.
<https://doi.org/10.1111/j.1365-2966.2010.17253.x>

- [9] Henriksen, M. and Byrd, G. (1996) Tidal Triggering of Star Formation by the Cluster Potential. *Astrophysical Journal*, **459**, 82. <https://doi.org/10.1086/176870>
- [10] Vijayaraghavan, R. and Ricker, P.M. (2017) The Co-Evolution of a Magnetized Intracluster Medium and Hot Galactic Coronae: Magnetic Field Amplification and Turbulence Generation. *Astrophysical Journal*, **841**, 38. <https://doi.org/10.3847/1538-4357/aa6eac>
- [11] Forman, W., *et al.* (1979) X-Ray Observations of Galaxies in the Virgo Cluster. *Astrophysical Journal*, **234**, L27. <https://doi.org/10.1086/183103>
- [12] Randall, S., *et al.* (2008) Chandra's View of the Ram Pressure Stripped Galaxy M86. *Astrophysical Journal*, **688**, 208. <https://doi.org/10.1086/592324>
- [13] Crowl, H. and Kenney, J. (2006) The Stellar Population of Stripped Cluster Spiral NGC 4522: A Local Analog to K+A Galaxies? *Astrophysical Journal*, **649**, L75. <https://doi.org/10.1086/508344>
- [14] Merluzzi, P., Busarello, G., Dopita, M.A., *et al.* (2013) ACCESS-V. Dissecting Ram-Pressure Stripping through Integral-Field Spectroscopy and Multiband Imaging. *Monthly Notices of the Royal Astronomical Society*, **429**, 1747. <https://doi.org/10.1093/mnras/sts466>
- [15] Kenney, J.-D., Geha, M., Jachym, P., Crowl, H., Dague, W., Chung, A., van Gorkom, J. and Vollmer, B. (2014) Transformation of a Virgo Cluster Dwarf Irregular Galaxy by Ram Pressure Stripping: IC3418 and Its Fireballs. *Astrophysical Journal*, **780**, 119. <https://doi.org/10.1088/0004-637X/780/2/119>
- [16] Gullieuszik, M., Poggianti, B.M., Moretti, A., *et al.* (2017) GASP. IV. A Muse View of Extreme Ram-Pressure-Stripping in the Plane of the Sky: The Case of Jellyfish Galaxy JO204. *Astrophysical Journal*, **846**, 27. <https://doi.org/10.3847/1538-4357/aa8322>
- [17] Roediger, E. and Bruggen, M. (2007) Ram Pressure Stripping of Disc Galaxies Orbiting in Clusters I. Mass and Radius of the Remaining Gas Disc. *Monthly Notices of the Royal Astronomical Society*, **380**, 1399. <https://doi.org/10.1111/j.1365-2966.2007.12241.x>
- [18] Tonnesen, S. and Bryan, G.-L. (2010) The Tail of the Stripped Gas That Cooled: HI, H, and X-Ray Observational Signatures of Ram Pressure Stripping. *Astrophysical Journal*, **709**, 1203. <https://doi.org/10.1088/0004-637X/709/2/1203>
- [19] Sun, M., Donahue, M. and Voit, G.-M. (2007) H Tail, Intracluster H II Regions, and Star Formation: ESO 137-001 in Abell 3627. *Astrophysical Journal*, **671**, 190. <https://doi.org/10.1086/522690>
- [20] Fumagalli, M., *et al.* (2014) MUSE Sneaks a Peek at Extreme Ram-Pressure Stripping Events I. A Kinematic Study of the Archetypal Galaxy ESO137-001. *Monthly Notices of the Royal Astronomical Society*, **445**, 4335. <https://doi.org/10.1093/mnras/stu2092>
- [21] Cortese, L., Gavazzi, G., Boselli, A., Franzetti, P., Kennicutt, R.C., O'Neil, K. and Sakai, S. (2006) Witnessing Galaxy Preprocessing in the Local Universe: The Case of a Star-Bursting Group Falling into Abell 1367. *Astronomy and Astrophysics*, **453**, 847. <https://doi.org/10.1051/0004-6361:20064873>
- [22] Kronberger, T., Kapferer, W., Ferrari, C., Unterguggenberger, S. and Schindler, S. (2008) On the Influence of Ram-Pressure Stripping on the Star Formation of Simulated Spiral Galaxies. *Astronomy and Astrophysics*, **481**, 337. <https://doi.org/10.1051/0004-6361:20078904>
- [23] Kapferer, W., Kronberger, T., Ferrari, C., Riser, T. and Schindler, S. (2008) On the

Influence of Ram-Pressure Stripping on Interacting Galaxies in Clusters. *Monthly Notices of the Royal Astronomical Society*, **bf389**, 1405.
<https://doi.org/10.1111/j.1365-2966.2008.13665.x>

- [24] Ramatsoku, M., *et al.* (2019) GASP XVII. HI Imaging of the Jellyfish Galaxy JO206: Gas Stripping and Enhanced Star Formation. *Monthly Notices of the Royal Astronomical Society*, **487**, 4580. <https://doi.org/10.1093/mnras/stz1609>
- [25] Owers, M.-S., Couch, W.-J., Nulsen, P.-E.-J. and Randall, S.-W. (2012) Shocking Tails in the Major Merger Abell 2744. *Astrophysical Journal*, **750**, L23.
<https://doi.org/10.1088/2041-8205/750/1/L23>
- [26] Ebling, H., Stephenson, L. and Edge, A.-C. (2014) Jellyfish: Evidence of Extreme Ram-Pressure Stripping in Massive Galaxy Clusters. *Astrophysical Journal*, **781**, L40. <https://doi.org/10.1088/2041-8205/781/2/L40>
- [27] Poggianti, B.-M., *et al.* (2016) Jellyfish Galaxy Candidates at Low Redshift. *Astronomical Journal*, **151**, 78. <https://doi.org/10.3847/0004-6256/151/3/78>
- [28] Koopmann, R. and Kenney, J. (2004) H α Morphologies and Environmental Effects in Virgo Cluster Spiral Galaxies. *ApJ*, **613**, 866. <https://doi.org/10.1086/423191>
- [29] Crowl, H. and Kenney, J. (2008) The Stellar Populations of Stripped Spiral Galaxies in the Virgo Cluster. *The Astrophysical Journal*, **136**, 1623.
<https://doi.org/10.1088/0004-6256/136/4/1623>
- [30] Tonnesen, S. and Bryan, G.L. (2012) Star Formation in Ram Pressure Stripped Galactic Tails. *Monthly Notices of the Royal Astronomical Society*, **422**, 1609.
<https://doi.org/10.1111/j.1365-2966.2012.20737.x>
- [31] Troncoso Iribarren, P., Padilla, N., Contreras, S., *et al.* (2016) Asymmetric Star Formation Efficiency Due to Ram Pressure Stripping. *Galaxy*, **4**, 77.
<https://doi.org/10.3390/galaxies4040077>
- [32] Bekki, K. (2014) Galactic Star Formation Enhanced and Quenched by Ram Pressure in Groups and Clusters. *Monthly Notices of the Royal Astronomical Society*, **438**, 444. <https://doi.org/10.1093/mnras/stt2216>
- [33] Steinhauser, D., Schindler, S. and Springel, V. (2016) Simulations of Ram-Pressure Stripping in Galaxy-Cluster Interactions. *Astronomy and Astrophysics*, **591**, A51.
<https://doi.org/10.1051/0004-6361/201527705>
- [34] Bekki, K. and Couch, W.J. (2003) Starbursts from the Strong Compression of Galactic Molecular Clouds Due to the High Pressure of the Intracluster Medium. *Astrophysical Journal*, **596**, L13. <https://doi.org/10.1086/379054>
- [35] Vulcani, B., *et al.* (2018) Enhanced Star Formation in Both Disks and Ram Pressure-Stripped Tails of GASP Jellyfish Galaxies. *Astrophysical Journal*, **866**, L25.
<https://doi.org/10.3847/2041-8213/aae68b>
- [36] Vijayaraghavan, R. and Ricker, P.M. (2013) Pre-Processing and Post-Processing in Group-Cluster Mergers. *Monthly Notices of the Royal Astronomical Society*, **435**, 2713. <https://doi.org/10.1093/mnras/stt1485>
- [37] McPartland, C., Ebling, H., Roediger, E. and Blumenthal, K. (2016) Jellyfish: The Origin and Distribution of Extreme Ram-Pressure Stripping Events in Massive Galaxy Clusters. *Monthly Notices of the Royal Astronomical Society*, **455**, 2994.
<https://doi.org/10.1093/mnras/stv2508>
- [38] Finoguenov, A., Henriksen, M.J., Miniati, F., Briel, U.G. and Jones, C. (2006) A Puzzling Merger in A3266: The Hydrodynamic Picture from Xmm-Newton. *Astrophysical Journal*, **643**, 790. <https://doi.org/10.1086/503285>
- [39] Henriksen, M.J. and Tittley, E.R. (2002) Chandra Observations of the A3266 Galaxy

- Cluster Merger. *Astrophysical Journal*, **577**, 701. <https://doi.org/10.1086/342115>
- [40] Henriksen, M., Donnelly, R.H. and Davis, D.S. (2000) Reconstructing the Merger History of the A3266 Galaxy Cluster. *Astrophysical Journal*, **529**, 692. <https://doi.org/10.1086/308295>
- [41] Dehghan, S., Johnston-Hollitt, M., Colless, M. and Miller, R. (2017) Dynamics of Abell 3266 I. An Optical View of a Complex Merging Cluster. *Monthly Notices of the Royal Astronomical Society*, **468**, 2645. <https://doi.org/10.1093/mnras/stx582>
- [42] De Grandi, S. and Molendi, S. (1999) A BEPOSAX Observation of the Merging Cluster Abell 3266. *Astrophysical Journal*, **527**, L25. <https://doi.org/10.1086/312393>
- [43] Cava, A., et al. (2009) WINGS-SPE Spectroscopy in the Wide-Field Nearby Galaxy-Cluster Survey. *Astronomy and Astrophysics*, **495**, 707. <https://doi.org/10.1051/0004-6361:200810997>
- [44] Fritz, J., et al. (2014) III. Equivalent Width Measurements, Spectral Properties, and Evolution of Local Cluster Galaxies. *Astronomy and Astrophysics*, **66**, 32. <https://doi.org/10.1051/0004-6361/201323138>
- [45] Kennicutt, R.C. (1998) Star Formation in Galaxies along the Hubble Sequence. *Annual Reviews of Astronomy and Astrophysics*, **36**, 189. <https://doi.org/10.1146/annurev.astro.36.1.189>
- [46] Hogg, D.W., Cohen, J.G., Blandford, R. and Pahre, M.A. (1998) The O II Luminosity Density of the Universe. *Astrophysical Journal*, **504**, 622. <https://doi.org/10.1086/306122>
- [47] Calzetti, D. (2012) Proceedings of the XXIII Canary Islands Winter School of Astrophysics: Secular Evolution of Galaxies.
- [48] Hasinger, G., Turner, T.J., George, I.M. and Boese, G. (1992) Legacy 2 (OGIP Calibration Memo CAL/ROS/92-001), 77.
- [49] Bekhti, N.-B., Floer, L., et al. (2016) HI4PI: A Full-Sky HI Survey Based on EBHIS and GASS. *Astronomy and Astrophysics*, **594**, A116. <https://doi.org/10.1051/0004-6361/201629178>
- [50] Kapferer, W., Sluka, C., Schindler, S., Ferrari, C. and Ziegler, B. (2009) The Effect of Ram Pressure on the Star Formation, Mass Distribution and Morphology of Galaxies. *Astronomy and Astrophysics*, **499**, 87. <https://doi.org/10.1051/0004-6361/200811551>
- [51] Abadi, M.G., Moore, B. and Bower, R.G. (1999) Ram Pressure Stripping of Spiral Galaxies in Clusters. *Monthly Notices of the Royal Astronomical Society*, **308**, 947. <https://doi.org/10.1046/j.1365-8711.1999.02715.x>
- [52] Miller, N. and Owen, F. (2003) ABELL 2255: Increased Star Formation and AGN Activity in a Cluster-Cluster Merger. *Astronomical Journal*, **125**, 2427. <https://doi.org/10.1086/374767>
- [53] Fritz, J., et al. (2011) WINGS-SPE II: A Catalog of Stellar Ages and Star Formation Histories, Stellar Masses and Dust Extinction Values for Local Clusters Galaxies. *Astronomy and Astrophysics*, **526**, 445. <https://doi.org/10.1051/0004-6361/201015214>
- [54] Fisher, D., Fabricant, D., Franx, M. and van Dokkum, P. (1998) A Spectroscopic Survey of the Galaxy Cluster CL 135862 ATz 0.328. *Astrophysical Journal*, **498**, 196. <https://doi.org/10.1086/305553>
- [55] Caldwell, N., Rose, J.A., Sharples, R.M., Ellis, R.S. and Bower, R.G. (1993) Star Formation in Early-Type Galaxies in the Coma Cluster. *Astronomical Journal*, **106**, 473. <https://doi.org/10.1086/116656>

- [56] Tran, K.H., Franx, M., Illingworth, G., Kelson, D.D. and van Dokkum, P. (2003) The Nature of E + A Galaxies in Intermediate-Redshift Clusters. *Astrophysical Journal*, **599**, 865. <https://doi.org/10.1086/379804>
- [57] Couch, W.J. and Sharples, R.M. (1987) A Spectroscopic Study of Three Rich Galaxy Clusters at $z = 0.31$. *Monthly Notices of the Royal Astronomical Society*, **229**, 423. <https://doi.org/10.1093/mnras/229.3.423>
- [58] Dressler, A., Smail, I., Poggianti, B., *et al.* (1999) A Spectroscopic Catalog of 10 Distant Rich Clusters of Galaxies. *Astrophysical Journal (Supplement)*, **122**, 51. <https://doi.org/10.1086/313213>
- [59] Freeland, E., *et al.* (2010) Quantifying the Importance of Ram-Pressure Stripping in a Galaxy Group at 100 Mpc. *Monthly Notices of the Royal Astronomical Society*, **409**, 1518. <https://doi.org/10.1111/j.1365-2966.2010.17379.x>
- [60] Wezgowiec, M., *et al.* (2012) NGC 3627: A Galaxy-Dwarf Collision. *Astronomy and Astrophysics*, **544**, 99. <https://doi.org/10.1051/0004-6361/201118436>
- [61] Vaughan, S., *et al.* (2020) K-CLASH: Strangulation and Ram Pressure Stripping in Galaxy Cluster Members at $0.3 < z < 0.6$. *Monthly Notices of the Royal Astronomical Society*, **496**, 3841. <https://doi.org/10.1093/mnras/staa1837>